Convergence of a Two-Level Ideal Algorithm for a Parametric Shape Optimization Model Problem

Benoît Chaigne, Jean-Antoine Désidéri

INSTITUT NATIONAL DE RECHERCHE EN INFORMATIQUE ET EN AUTOMATIQUE

Convergence of a Two-Level Ideal Algorithm for a Parametric Shape Optimization Model Problem

Benoît Chaigne — Jean-Antoine Désidéri

N° 7068 — version 2

initial version September 2009 — revised version September 2009

Thème NUM

ISSN 0249-6399 ISRN INRIA/RR--7068--FR+ENG

INSTITUT NATIONAL
DE RECHERCHE
EN INFORMATIQUE
ET EN AUTOMATIQUE

INRIA

centre de recherche
SOPHIA ANTIPOLIS - MÉDITERRANÉE

Convergence of a Two-Level Ideal Algorithm for a Parametric Shape Optimization Model Problem

Benoît Chaigne, Jean-Antoine Désidéri

Thème NUM — Systèmes numériques
Équipe-Projet Opale

Rapport de recherche n° 7068 — version 2 — initial version September 2009 — revised version September 2009 — 66 pages

Abstract: The numerical approximation of the solution of a PDE is generally obtained with the resolution of a system of equations (linear or nonlinear) that comes from the discretization of the PDE on a given domain. The resulting system may be stiff, partly due to the approximation of differential operators, and therefore makes the iterative methods harder to converge. In order to overcome this difficulty, the classical (or geometrical) multigrid strategies aim at preconditioning this system through the use of coarser representations (grids). Equivalently, the numerical treatment of an optimization problem is potentially subject to stiffness difficulties. In the framework of a parametric shape optimization problem, hierarchical representations can be used to enhance the multilevel strategies to this context. In this paper, by analogy with the Poisson equation (elliptic linear PDE), which is the typical example for linear multigrid methods, we address a convex parametric shape optimization model problem. We describe the ideal cycle of a two-level algorithm adapted to shape optimization problems relying on appropriate transfer operators (prolongation and restriction). The efficiency of a multigrid strategy is ensured by a mesh-independent convergence rate. With the help of a symbolic calculus software we show that this is indeed the case (we derive a convergence rate which is independent of the dimension of the parametric representation). Moreover this rate is "small" (smaller than the convergence rate of basic iterative methods such as Jacobi, Gauss-Seidl, etc.). Numerical examples are worked out and corroborate the theoretical results.

Key-words: shape optimization, inverse problem, multigrid methods, convergence rate

Centre de recherche INRIA Sophia Antipolis – Méditerranée
2004, route des Lucioles, BP 93, 06902 Sophia Antipolis Cedex
Téléphone : +33 4 92 38 77 77 — Télécopie : +33 4 92 38 77 65

Convergence d'un algorithme bigrille idéal pour un problème modèle d'optimisation de forme paramétrique

Résumé : Une approximation numérique de la solution d'une EDP s'obtient en général en résolvant un système d'équations (linéaires ou non-linéaires) provenant de la discrétisation de cette EDP sur un domaine. La raideur du système obtenu, en partie due à l'approximation d'opérateurs différentiels, handicape les méthodes itératives de résolution. En réponse à cette difficulté, les stratégies multigrilles classiques (ou géométriques) ont pour fonction de préconditionner ce système au moyen de discrétisations (grilles) grossières. Au même titre que pour la résolution itérative d'un système d'équations, le traitement numérique d'un problème d'optimisation est potentiellement soumis à des problèmes de raideur. Dans le cadre d'un problème d'optimisation de forme paramétrique, des représentations hiérarchiques existent permettant d'étendre les stratégies multiniveaux au contexte de l'optimisation. Dans ce papier, par analogie à l'équation de Poisson (EDP elliptique linéaire) qui est le problème typique des méthodes multigrilles linéaires, on propose de traiter un problème modèle convexe d'optimisation de forme paramétrique. On décrit et on analyse la convergence du cycle idéal d'un algorithme bigrille adapté à l'optimisation de forme grâce à la définition d'opérateurs de transfert (prolongement et restriction) adéquats. L'efficacité d'une stratégie multigrille se traduit par un taux de convergence indépendant du maillage. À l'aide d'un outil de calcul symbolique on montre que c'est effectivement le cas (le taux de convergence est indépendant de la dimension de la représentation paramétrique) et que ce taux est "petit" (plus petit que le taux de convergence des méthodes classiques telles que Jacobi). Des exemples numériques illustrent et confirment ces résultats.

Mots-clés : optimisation de forme, problème inverse, méthodes multigrilles, taux de convergence

Contents

1 Introduction

Many engineering problems are defined as inverse problems: one wants to optimize a device such that a certain physically relevant target function is attained (or approached as close as it is physically possible). This function depends one a state variable governed by the partial differential equations (PDE) of the underlying physics. When the control is the geometry of the device, which is commonly the case, the inverse problem reads as the following shape functional

$$\min_{\mathcal{S}} \mathcal{J}(\mathcal{S}) = \int_{\Omega} \left\| \mathcal{O}(u(\mathcal{S}), \omega) - \tilde{\mathcal{O}}(\omega) \right\|^2$$

where $\mathcal{S}$ belongs to some feasible class of shapes. As for PDE, the numerical treatment of such problems can be difficult due to numerical stiffness, which increases with the design space dimension. Among other preconditioning techniques, Multilevel/Multigrid (MG) methods are often used to overcome this difficulty. MG methods for solving PDE have been widely studied in the past years. Introduced by Fedorenko [11, 12] for solving linear PDE such as the Poisson equation, they are now successfully used for large nonlinear systems with *Full Approximation Scheme* (FAS) or Newton approaches [3, 13, 25, 7, 4]. Originally based on hierarchical discrete representations of the domain, they have been extended to a purely algebraic approach known as *Algebraic Multigrid* (AMG) [23]. More recently, several algorithms have been proposed to enhance the MG methods to the framework of PDE-constrained shape optimization problems. Among them we find the *consistent approximations* of Polak [22, 19, 21], the *one-shot* methods, the MG/Opt algorithm, as well as parametric approaches [18]. A rather complete bibliography can be found in [2].

The *consistent approximations* technique provides a proof for the convergence of successive discrete solutions towards the continuous one under consistent hypothesis. The resulting algorithm is a gradient-based *Nested Iteration* algorithm. Assuming that an iterative method is used to compute the PDE and its adjoint, the Polak algorithm takes also into account possible incomplete calculations (that is, within a given finite number of iterations, whatever the remaining residual). This means that we do not actually need the exact values to obtain a descent direction, thus reducing the cost of the calculation.

The so-called *one-shot* methods intend to solve in a single iterative process both the system of state equations and the necessary optimality conditions. The overall system being nonlinear, a FAS- or Newton-like strategy is applied [16, 1, 17, 24, 9]. This strategy turns out to be irrelevant when the state is an explicit function of the geometry or when the state equation is a linear system solved by a direct method (Gauss, Cholesky).

The MG/Opt algorithm is a shape optimization algorithm developed by Nash *et. al* [20, 14, 15] inspired by the nonlinear MG algorithm FAS. It is based on the hierarchy of approximation spaces of the state variable (not necessarily of the shape representation). The approximation spaces are usually defined together with the mesh (*e.g.* P1 elements on a triangulated surface). Since the cost function depends on the state, there exists a mapping between h, the characteristic mesh size, and J_h, the corresponding approximated cost function. In other words, a hierarchy in terms of approximation spaces of the state implies a hierarchy in terms of approximations of J, whatever the shape representation (CAD-free or parametric). In order to ensure the consistency between the functions J_h to be minimized, a FAS strategy is used: thus, a descent direction on a coarse is a descent direction on the fine grid.

In a parametric representation, the design space and the discrete representation for the calculus of the cost function are independent. In this article we assume that this latter remains fixed and we focus on the hierarchy of the parametric design spaces. In that case, since the objective function to be minimized is the same for each level of the design space, the consistency between the "grids" is achieved. In order to show why MG-like algorithms are very different in the framework of shape inverse/optimization problems we consider two-level ideal algorithms applied to a simple parametric shape inverse problem. Using the terminology of the MG theory we propose a convergence proof. As an ideal algorithm, we assume that the coarse problem is solved exactly. In addition, the relaxation method is a simple steepest descent method. For different transfer operators the convergence rate of the ideal cycle is derived. Depending on these operators, the convergence rate turns out to be independent of the search space dimension or not. Numerical examples illustrate the fundamental differences between PDE and shape optimization.

The outline is the following: in section 2 we set the optimization problem and we report connections with the Poisson equation, particularly through a spectral analysis; then, in section 3, we recall important results on the convergence of linear iterations and the concept of smoothing; in section 4 we deal with the two-level algorithms and the transfer operators; in section 4.4 we illustrate the theoretical results with numerical example and in section 5 we extend the problem to CAD parameterization; finally we draw some conclusions and suggest perspectives in section 6.

2 Definition of the model problems

We consider the best approximation problem of a real-valued function $\bar{u}$ of $L_2([0\ 1])$ in a finite-dimensional subspace. This problem will be referred in the sequel as the shape optimization problem. We will see that it is closely related to the Poisson equation $-\Delta u = f$, which is the typical model problem for linear MG methods. In their discrete formulations, both problems lead to symmetrical linear systems. We exhibit the eigen-decomposition of both matrices.

2.1 Best approximation

Let H_0 be the Hilbert space of L_2 functions defined on the interval $[0\ 1]$ such that $u(0) = u(1) = 0$ with the inner product

$$(u, v) = \int_0^1 u(t)v(t)dt \tag{1}$$

and the associated norm

$$\|u\| = \sqrt{(u, u)} = \left(\int_0^1 |u(t)|^2 \, dt \right)^{1/2}. \tag{2}$$

2.1.1 Shape functional

Let $\bar{u}$ be a function in H_0 and F a subspace of H_0. The best approximation of $\bar{u}$ in F reads as the minimization of the L_2 norm of the difference between $u \in F$ and the target function $\bar{u}$, that is:

$$\min_{u \in F} \mathcal{J}(u) = \frac{1}{2} \|u - \bar{u}\|^2 = \frac{1}{2} \int_0^1 |u(t) - \bar{u}(t)|^2 \, dt. \tag{3}$$

$\mathcal{J}$ is obviously continuous, differentiable and quadratic (hence convex). Let $\mathcal{G}$ be the differential:

$$\langle \mathcal{G}(u), \delta u \rangle = (u - \bar{u}, \delta u) = \int_0^1 \big(u(t) - \bar{u}(t)\big)\delta u(t)dt, \quad \forall \delta u \in H_0 \tag{4}$$

and $\mathcal{H}$ the Hessian:

$$\langle \mathcal{H}(f)\delta u, \delta v \rangle = (\delta u, \delta v) = \int_0^1 \delta u(t)\delta v(t)dt, \quad \forall \delta u, \delta v \in H_0. \tag{5}$$

Since $\mathcal{J}$ is quadratic, $\mathcal{H}$ does not depend on u and is positive definite:

$$\langle \mathcal{H}(u)\delta u, \delta u \rangle = \|\delta u\|^2 > 0, \qquad \forall u, \forall \delta u \neq 0$$

2.1.2 Parametric functional

The parametric approach consists in approaching $\bar{u}$ in a finite-dimensional space F. Let $\{u_k\}_{k=1}^N$ be a free family of functions in H_0. The space $F = \mathrm{span}\{\dots, u_k, \dots\}$ is a subspace of H_0 of dimension N (or equivalently of degree $N - 1$ for polynomial spaces).

A function u of F is noted $u[x]$ where x is the vector of coefficients[1] $x \in \mathbb{R}^N$ in the basis $\{u_k\}_{k=1}^N$, that is,

$$u[x](t) = \sum_{k=1}^{N} x_k u_k(t). \tag{6}$$

Injecting the representation (6) of u in (3) yields

$$\forall u \in F, \quad \mathcal{J}(u) = \frac{1}{2}\int_0^1 \left| \sum_{k=1}^{N} x_k u_k(t) - \bar{u}(t) \right|^2 dt.$$

The parametric functional is the following finite-dimensional application defined on $\mathbb{R}^N$:

$$J(x) \stackrel{\text{def.}}{=} \mathcal{J}(u[x]) \tag{7}$$

which is merely the expression of the shape functional (3) defined on the subspace F in terms of the design parameters x. Note that the parametric functional essentially relies on the search space basis which is not unique. For a given subspace the choice of the basis may be critical. Namely, it can yield bad numerical properties for the convergence of numerical optimization algorithms (in particular slow convergence related to the conditioning). We will come to that later when dealing with the multilevel algorithms.

The gradient G of J is

$$G(x) = \begin{pmatrix} \vdots \\ \langle \mathcal{G}(u[x]), u_k \rangle \\ \vdots \end{pmatrix}, \tag{8}$$

and the Hessian H is

$$H(x) = \begin{pmatrix} & \vdots & \\ \cdots & \langle \mathcal{H}(u[x])u_k, u_j \rangle & \\ & & \end{pmatrix}. \tag{9}$$

In a simpler way, the parametric functional reads as the quadratic form:

$$J(x) = \frac{1}{2} x^T H x - b^T x + c \tag{10}$$

where $b_k = (\bar{u}, u_k)$ and $c = \frac{1}{2}\|\bar{u}\|^2$. Note that H is still s.p.d. for the same reason that $\mathcal{H}$ is s.p.d. In that case the necessary optimality condition $G(x) = 0 \Leftrightarrow Hx - b = 0$ implies that the problem (3) is equivalent to solving the linear system $Hx = b$. Numerical properties of the problem can be investigated studying the Hessian H whose elements h_{kj} are

$$h_{kj} = \int_0^1 u_k(t) u_j(t) dt \tag{11}$$

in the basis $\{u_k\}_{k=1}^N$.

2.1.3 Application with P1 elements

Let us consider P1 elements as approximation space of $\bar{u}$. That is, we aim at approaching $\bar{u}$ with a piecewise linear function (This approach is considered as CAD-free in the sense that it relies on a mesh $\mathcal{T}_h$, contrary to Bézier representations or other meshless parameterizations, see section 5).

[1] In the CAD terminology, the coefficients x are also called *control points*, which makes sense for Bézier or B-spline curves and more generally for NURBS.

Let $\mathcal{T}_h$ be a uniform discretization of the interval $[0\ 1]$: $t_k = kh$, $h = \frac{1}{N+1}$, $k = 0, \ldots, N+1$. The P1 functions ("hat" functions, see Figure 1) are defined by

$$u_k(t) = \begin{cases} \frac{t-t_{k-1}}{h} & t \in [t_{k-1}\ t_k] \quad k > 0 \\ \frac{t_{k+1}-t}{h} & t \in [t_k\ t_{k+1}] \quad k < N+1 \\ 0 & t \notin [t_{k-1}\ t_{k+1}] \end{cases} . \tag{12}$$

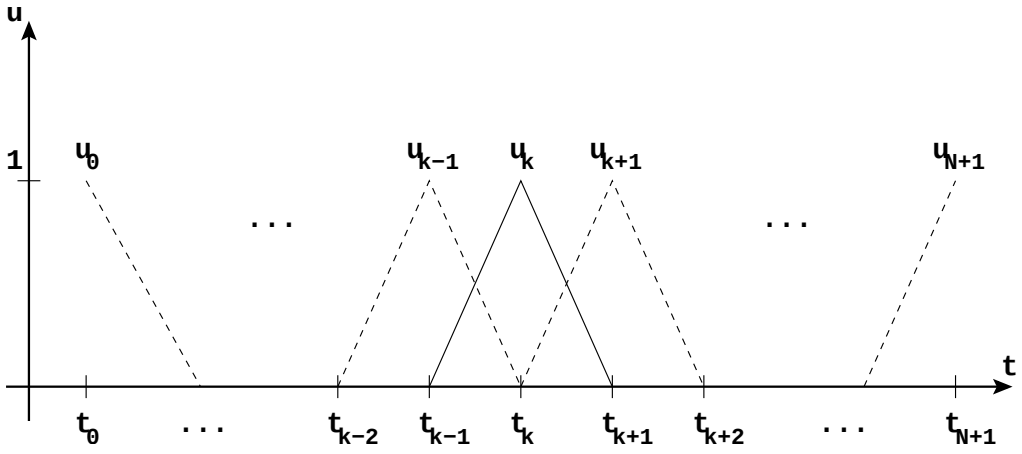

Figure 1: P1 elements of $\mathcal{T}_h$

The local support of the functions u_k implies that the Hessian matrix, noted H_h, has a band structure. With linear approximation the bandwidth is 3:

$$h_{jk} = \begin{cases} \int_0^h \left(\frac{t}{h}\right)^2 dt & = & \frac{h}{3} & j = k = 0,\ j = k = N+1 \\ 2\int_0^h \left(\frac{t}{h}\right)^2 dt & = & \frac{2h}{3} & 0 < j = k < N+1 \\ \int_0^h \frac{t}{h}\left(1 - \frac{t}{h}\right) dt & = & \frac{h}{6} & j = k+1,\ j = k-1 \end{cases} . \tag{13}$$

Hence we have $H_h = \frac{h}{6} B$ with

$$B = \begin{pmatrix} 4 & 1 & & & \\ 1 & 4 & 1 & & \\ & \ddots & \ddots & \ddots & \\ & & 1 & 4 & 1 \\ & & & 1 & 4 \end{pmatrix} \in \mathbb{R}^{N \times N} \tag{14}$$

where we have applied Dirichlet boundary conditions (*i.e.* we have ignored the functions u_0 and u_{N+1}). The right-hand side (RHS) b_h is given by $(b_h)_k = (\bar{u}, u_k)$.

B is a real symmetric matrix. As such it admits an orthogonal diagonalization $B = \Omega\Lambda\Omega^T$ with real eigenvalues. Moreover B is strictly diagonally dominant. According to the Gershgorin theorem the spectrum of B is such that $\sigma(B) \subset [2\ 6]$. Consequently the condition number of B is bounded by $\kappa_2 \leq 3$, whatever the mesh size N.

2.2 Poisson equation

The 1D Poisson equation on the closed interval $[0\ 1]$ with homogeneous Dirichlet boundary conditions reads

$$\begin{cases} -u''(t) = f(t) & t \in]0\ 1[\\ u(0) = u(1) = 0 \end{cases} \tag{15}$$

for some given function f. Let us consider the following centered finite differences scheme to approach the second derivative:

$$-u''(t) = \frac{-u(t-h) + 2u(t) - u(t+h)}{h^2} + O(h^2). \tag{16}$$

Evaluating this approximation at the nodes t_k of the uniform mesh $\mathcal{T}_h$ yields the linear system $A_h u_h = f_h$ where

$$A_h = \frac{1}{h^2} A = \frac{1}{h^2} \begin{pmatrix} 2 & -1 & & & & \\ -1 & 2 & -1 & & & \\ & \ddots & \ddots & \ddots & & \\ & & & -1 & 2 & -1 \\ & & & & -1 & 2 \end{pmatrix} \in \mathbb{R}^{N \times N}, \tag{17}$$

$(u_h)_k = u(t_k)$ and $(f_h)_k = f(t_k)$.

A is a real symmetric matrix: it has an orthogonal diagonalization $A = S \Pi S^T$ with real eigenvalues. Moreover, according to the Gershgorin theorem, the spectrum of A is such that $\sigma(A) \in [0\ 4]$.

2.3 Spectral analysis

The previously defined model problems lead to the linear systems $H_h x = b_h$ and $A_h u_h = f_h$. Before devising on the numerical treatment for solving these equations, let us discuss the eigenstructure of H_h and A_h.

We have seen that $H_h = \frac{h}{6} B$ and $A_h = \frac{1}{h^2} A$ where A and B do not depend on the mesh size h. It is easy to verify that both model problems are strongly related by the following relation

$$B = 6I - A. \tag{18}$$

Hence the diagonalization of B is closely related to that of A:

$$\Omega = S \tag{19}$$

$$\Lambda = 6I - \Pi \tag{20}$$

Both matrices have the same eigenvectors associated to eigenvalues which are inversely ordered and shifted. More precisely, assume without loss of generality (w.l.o.g.) that the eigenvalues of A, noted μ_k, are increasingly ordered:

$$0 < \mu_1 < \cdots < \mu_N < 4. \tag{21}$$

Hence the eigenvalues of B, noted λ_k, are

$$\lambda_k = 6 - \mu_k \quad \Longrightarrow \quad 6 > \lambda_1 > \cdots > \lambda_N > 2. \tag{22}$$

The diagonalization of A is well known (see [7, 6] *e.g.*): if S_k denotes the kth eigenvector associated to μ_k we have

$$S_k = \sqrt{2h} \begin{pmatrix} \vdots \\ \sin(jk\pi h) \\ \vdots \end{pmatrix}, \quad \mu_k = 2 - 2\cos(k\pi h). \tag{23}$$

Remark 1. *It is straightforward to check that the spectrum of A and B lie in the intervals predicted by the Gershgorin theorem. In addition the inequalities of* (21) *and* (22) *are strict. Hence $\kappa_2(B) < 3$.*

Remark 2. *Ω is both symmetrical and orthogonal, i.e. $\Omega = \Omega^T = \Omega^{-1}$.*

The eigenvectors (see Figure 2) are discrete Fourier modes on $\mathcal{T}_h$ (the coefficient $\sqrt{2h}$ is a normalization coefficient). Each eigenvector is characterized by a frequency parameter $\theta_k = k\pi h$. We refer to *high*

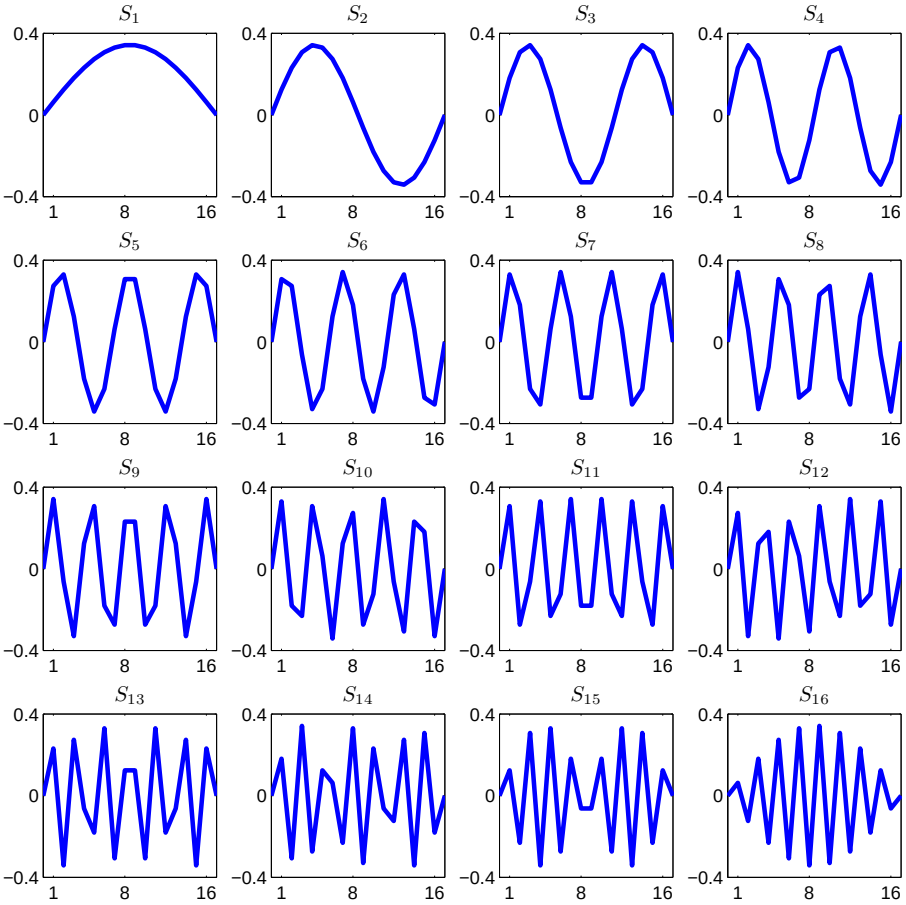

Figure 2: Eigenvectors of A and B: discrete Fourier modes ($N = 16$)

frequency modes (HF) the eigenvectors S_k such that $\theta_k \geq \frac{\pi}{2}$ and to *low frequency modes* (LF) the remaining eigenvectors, satisfying $\theta_k < \frac{\pi}{2}$.

Using the terminology introduced above, the two model problems can be set apart according to their eigenstructure: the low frequency modes are associated to the smallest eigenvalues in the case of the Poisson equation; they are associated to the largest eigenvalues in the case of the best approximation problem. Symmetrically, the high frequency modes are associated to the largest eigenvalues in the case of the Poisson equation whereas they are associated to the smallest eigenvalues in the case of the best approximation problem (see Figure 3).

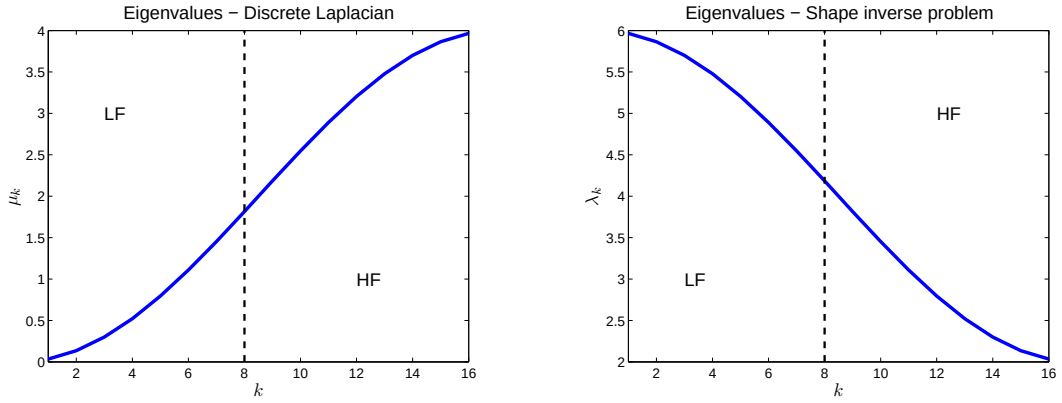

(a) $\sigma(A)$ (b) $\sigma(B)$

Figure 3: Eigenvalues of A and B

In accordance with this structure the linear operators A_h and H_h have opposite smoothing properties. Indeed, a matrix-vector product amplifies the modes of largest eigenvalues (the LF or HF modes depending on the problem). In the style of [15], a simple manner to illustrate that a linear operator M is a smoother (or an "anti-smoother") is to look at the discrete Fourier transform (DFT) of the Krylov vectors $q^i = M^i x$ for some vector x (assumed to be non zero in the direction of each eigenvector). An example is given in the Figure 4. In compliance with their eigenstructure, A_h (or A) amplifies the HF components and H_h (or B) amplifies the LF components.

The analytical knowledge of the diagonalization of B will be useful for the convergence study of the two-grid ideal schemes. Anticipating the sequel, one can already realize that a classical MG strategy (in the sense of a PDE-like strategy) will fail in this framework: we lack a smoother operator. In order to explain this argument in details we will review in the section 3 the decay properties of basic iterative methods, focusing on the optimization point of view.

Remark 3. *The MG methods are efficient for stiff linear systems; the best approximation problem in the P1 parameterization is however well-conditioned ($\kappa_2 < 3$). In the section 5 we will generalize this problem to a parametric optimization problem (mesh-independent parameterization, i.e. without using $\mathcal{T}_h$). At this occasion we will show that the condition number can become pathologically high as the space dimension increases.*

2.4 Relevance of the shape optimization model problem

We can argue the fact that the shape optimization model problem may be irrelevant for more complex situations of shape optimization/inverse problems. In particular we have in mind the optimal design of some engineering device w.r.t. a criterion that depends on a state variable governed by a PDE. In that case one has to take care of the sensitivity of the state w.r.t. shape deformations.

First, there is no specific reason for the criterion to be a quadratic function of the design variables, nor a convex one. Hence the necessary optimality conditions have to be reached through a non-linear process. In

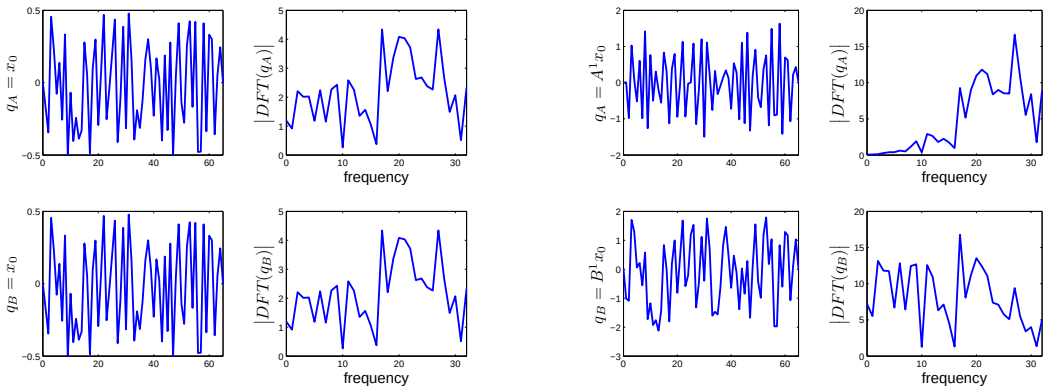

(a) $i = 0$ (b) $i = 1$

(c) $i = 5$ (d) $i = 10$

Figure 4: Krylov vectors q_A^i and q_B^i where $q_A^0 = q_B^0 = v_h = b_h$ is a random vector and $N = 64$. The DFT of the initial vector exhibits an approximately uniform distribution of the frequencies. After one iteration, the HF components of q_B^1 seem to be less amplified than the other (from 20 to 30); similarly, the LF components of q_A^1 are less amplified. After 5 and 10 iterations only half of the components remains observable: the LF modes for q_B^i and the HF modes for q_A^i.

other words, the Hessian matrix is not constant and may not be positive definite at any point. Concerning this last point we can restrict our study to a local point of view: since the Hessian matrix need be positive definite at the point of a local minimum, assuming enough regularity on the criterion, there exists a vicinity where the Hessian remains positive definite.

Nevertheless, apart from the positivity of the eigenvalues, nothing can be said *a priori* about the spectral structure of the Hessian in this vicinity. It has however been observed numerically for some cases that the Hessian exhibits a spectral structure similar to that of the model problem. More precisely, it has been encountered for the parametric shape optimal design of a reflector antenna [5].

3 Review of basic iterative methods

In this section we consider basic iterative methods for solving the linear system $Mx = b$ or equivalently minimizing the function $\frac{1}{2}x^T Mx - b^T x$ when M is symmetric positive definite, namely the *Jacobi method* and the *steepest descent method*. We first recall fundamental results about the convergence of linear iterations (for more details we refer the reader to [6] for instance). Their application to the model problems will be considered in the last subsection.

3.1 Linear iteration: generalities

First let us introduce generalities on sequences generated by linear iterations. A linear iteration takes the following form

$$x^{i+1} = Gx^i + b \tag{24}$$

where G is called the amplification matrix. A necessary and sufficient condition for the sequence (24) to converge is that the spectral radius of G, noted $\rho(G)$, must be strictly less than 1. Let us assume that this is true. Let x^* be the fixed point and $e^i = x^i - x^*$ the iterative error. Since x^* verifies $x^* = Gx^* + b$ we deduce the following relation between e^i and e^{i+1}

$$e^{i+1} = Ge^i, \tag{25}$$

which tells that one iteration amplifies the error by G.

Assume further that G is diagonalizable. Let $G = T\Gamma T^{-1}$ with $\Gamma = diag(0 < |g_1| \leq \cdots \leq |g_n| < 1)$. The columns of T are eigenvectors associated to the eigenvalues g_k. Hence we have

$$\begin{aligned} T^{-1}e^{i+1} &= \Gamma T^{-1}e^i \\ \epsilon^{i+1} &= \Gamma\epsilon^i \end{aligned}$$

where $T\epsilon^i = e^i$. That is, ϵ^i is the error in the modal basis T. One linear iteration corresponds to the decay of the error by a factor $|g_k|$ in the direction of the corresponding eigenvector

$$\epsilon_k^{i+1} = g_k\epsilon_k^i. \tag{26}$$

These coefficients g_k are called *decay factors*. Their absolute value can be taken as componentwise rates of convergence. The global convergence rate of the iteration is given by the spectral radius $\rho = \max_k |g_k|$, *i.e.* the decay factor of largest magnitude.

Let us now examine two linear iterative methods for solving the same problem from two points of view: as a system of linear equations (Jacobi method) or as the minimization of a quadratic form (steepest descent method). We derive their amplification matrices.

3.2 Jacobi iteration

The Jacobi method for solving a linear system $Mx = b$ reads

$$x^{i+1} = \left(I - D_M^{-1}M\right)x^i + D_M^{-1}b \tag{27}$$

where D_M is the diagonal part of M. Introducing the relaxation parameter τ yields

$$x^{i+1} = \left(I - \tau D_M^{-1} M\right) x^i + \tau D_M^{-1} b. \tag{28}$$

Assuming w.l.o.g. that the system has already been scaled such that the diagonal of M is the identity, the amplification matrix of the Jacobi iteration with relaxation parameter τ reads

$$G_\tau = I - \tau M. \tag{29}$$

More generally, after k Jacobi iterations with coefficients $\tau_j,\ j = 1 \dots k$, the amplification matrix reads

$$G_k = (I - \tau_k M) \cdots (I - \tau_1 M). \tag{30}$$

Remark 4. *The coefficients τ_j can be chosen in a smart way to reduce the error in the direction of the modes corresponding to a given subset of the spectrum. This method is known as the* Richardson iteration *or the* Tchebychev acceleration method*.*

3.3 Steepest descent method

We consider a finite-dimensional quadratic functional J with s.p.d. Hessian matrix M. The gradient of J reads

$$J'(x) = Mx - b. \tag{31}$$

The application of the steepest descent method to minimize J consists in the following linear iteration

$$\begin{aligned} x^{i+1} &= x^i - \tau J'(x^i) \\ &= x^i - \tau(Mx^i - b) \\ &= (I - \tau M)x^i + \tau b \end{aligned}$$

where the step τ can either be fixed or given by a line search along the gradient direction $Mx^i - b$.

It appears that the steepest descent iteration with step τ can be seen as a Jacobi iteration with relaxation parameter τ if the problem has been properly scaled beforehand (*i.e.* the diagonal of M is the identity). Consequently, the amplification matrix is equivalent to (29) for one descent iteration and equivalent to (30) for k descent iterations.

3.4 Decay functions of the basic methods applied to the model problems

Now that we have set the equivalence between a Jacobi iteration and a steepest descent iteration, let us apply this method to both model problems in order to derive the decay factors. This will provide useful information about the iterative convergence [2].

Let us assume that both problems are scaled, *i.e.*

$$D_A^{-1} A_h f_h = D_A^{-1} v_h$$

$$D_B^{-1} H_h x_h = D_B^{-1} b_h.$$

Hence the amplification matrices reads

$$G_\tau^A = I - \tfrac{\tau}{2} A$$

$$G_\tau^B = I - \tfrac{\tau}{4} B.$$

According to the section 2.3 both matrices are diagonalizable and the decay factors read

$$g_k^A = 1 - \tfrac{\tau}{2}\mu_k$$

$$g_k^B = 1 - \tfrac{\tau}{4}\lambda_k.$$

[2] The study of the Jacobi method applied to the Poisson equation is a well-known problem. We recall it for a sake of comparison with the shape optimization problem.

The Figure 5 depicts the decay functions (*i.e.* the decay factors w.r.t. the mode indexes) for different values of the parameter τ.

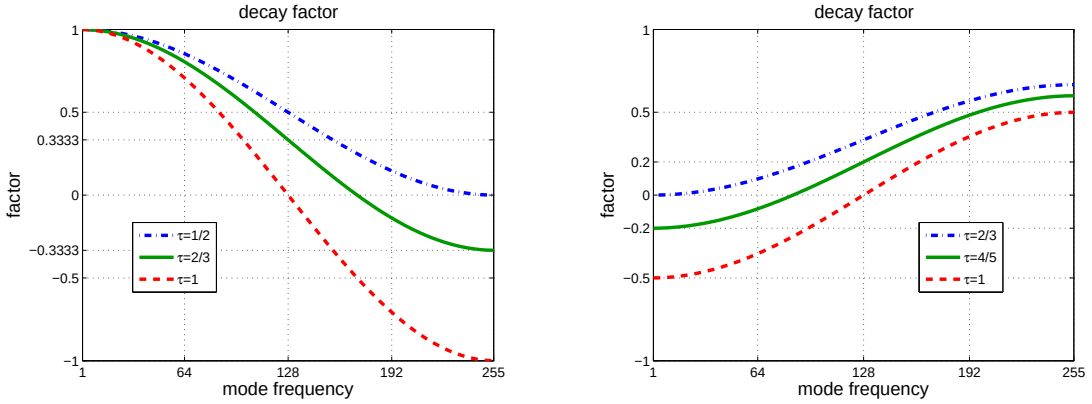

(a) Poisson equation

(b) best approximation

Figure 5: Decay function of one Jacobi (steepest descent) iteration for some values of the relaxation parameter τ and for $N = 255$

According to the Figure 5, the convergence is faster in the direction of some modes. More precisely, recalling that the modes are discrete Fourier modes, the decay functions are monotonous functions of the frequency mode: it is decreasing in the case of the Poisson equation and increasing in the case of the shape optimization problem.

Provided that all decay factors remain in $]-1\ 1[$ for the sake of convergence, the relaxation parameter τ can be set to modify the decay function. Ideally, one would optimize τ such that the spectral radius is minimized. However, in a stiff problem such as the discrete Poisson equation, the smallest eigenvalue remains close to one, whatever the value of τ. Alternatively, it may be more relevant to optimize τ on a subset of the space rather than globally. In the sequel we divide the search space into two complementary subspaces: the subspace spanned by the LF eigenmodes and the subspace spanned by the HF eigenmodes, identified respectively by the subset of indexes I_{LF} and I_{HF} (assuming that N is odd)

$$I_{LF} = \left\{1, \cdots, \frac{N-1}{2}\right\} \qquad I_{HF} = \left\{\frac{N+1}{2}, \cdots, N\right\}.$$

In the following subsections we provide the optimal value of τ that minimizes one of the following criterions

$$\rho = \max_{k \in I_{LF} \cup I_{HF}} |g_k| \qquad \rho_{LF} = \max_{k \in I_{LF}} |g_k| \qquad \rho_{HF} = \max_{k \in I_{HF}} |g_k|$$

in accordance with each problem.

3.4.1 Optimal relaxation parameter for the Poisson equation

First note that the method converges only when τ lies in the interval $]0\ 1]$. This ensures that all decay factors are such that $\left|g_k^A\right| < 1$.

For all τ in $]0\ 1]$, the decay factors are positive in the LF part. Since the decay function is monotonous decreasing w.r.t. k, the decay factor of maximum absolute value is $g_1^A = 1 - \tau + \tau \cos \pi h$ which is minimized for $\tau = 1$, yielding $\rho_{LF} = \cos \pi h$. This means that the iteration cannot be efficient on the LF part, unless h is large enough (*i.e.* N must be small: the parameterization/grid is coarse). Since ρ is necessarily greater or equal than ρ_{LF} (here $\rho = \rho_{LF}$) it makes no sense to optimize τ globally.

On the contrary, τ can be set to minimize ρ_{HF}. In that sense the optimal value is $\tau = \frac{2}{3}$ for which the largest decay factor is obtained at $k = \frac{N+1}{2}$ and equal to $\frac{1}{3}$. Note that this value is independent of the mesh

size. In the Multigrid terminology this method is called a *smoother* since it reduces efficiently the HF part of the error. In the literature, the smoother is sometimes called the *solution operator*.

With this value the decay factors read

$$g_k^A = \frac{1}{3}\left(1+2\cos(k\pi h)\right)$$

Hence the spectral radius of the amplification matrix equivalent to n Jacobi iterations is

$$\begin{aligned}\rho(G_n^A) &= \frac{1}{3^n}\max_k\left|\left(1+2\cos(k\pi h)\right)^n\right| \\ &= \frac{1}{3^n}\left(\max_k\left|1+2\cos(k\pi h)\right|\right)^n \\ &= \frac{1}{3^n}\left(1+2\cos(\pi h)\right)^n\end{aligned}$$

3.4.2 Optimal relaxation parameter for the shape inverse problem

In this case the convergence of the method requires that τ lies in $]0\ \frac{4}{3}]$ (allowing τ to be an over-relaxation parameter). The main difference with the previous problem is that τ can be set efficiently for either the LF or the HF part. This comes from the fact that no eigenvalue is close to zero. In other words this problem is well conditioned.

From a global point of view, the optimal value to minimize ρ is obtained at $\tau = 1$ and yields $\rho = \frac{1}{2}\cos(\pi h)$, which is mesh dependent but bounded from above by $\frac{1}{2}$. This defines the global best solution operator. On the HF part, the optimal value is $\rho_{HF} = \frac{1}{3}(2\cos(\pi h) - 1)$ and reached at $\tau = \frac{4}{3}$, which is also mesh size dependent, though bounded from above by $\frac{1}{3}$.

We will assume in this article that none of these configurations is a choice we can do. The first argument for this statement is that other parameterization, such as the Bézier-Bernstein parameterization, can lead to stiff problems (the lowest eigenvalue is close to 0, see [8]). In that case τ can be optimally set to minimize ρ_{LF} (the solution operator is a good *anti-smoother*) but no value of τ can be set in order to reduce efficiently the error on the HF part (and consequently no τ can be set to reduce ρ significantly): this is numerically illustrated in the section 5. But in that specific case we do not have any closed form for the spectrum and consequently we cannot conduct a rigorous analysis of the convergence of the proposed multilevel methods in the section 4.

The second argument is that the best solution operator on the LF part is more efficient than the best solution operator on the HF part. Indeed the optimal value is $\rho_{LF} = \frac{1}{5}$ (mesh independent) and reached at $\tau = \frac{4}{5}$. In this configuration the decay factors read

$$g_k^B = \frac{1}{5}\left(1-2\cos\left(k\pi h\right)\right)$$

Thus, the spectral radius of the amplification matrix equivalent to n Jacobi iterations is

$$\begin{aligned}\rho(G_n^B) &= \frac{1}{5^n}\max_k\left|\left(1-2\cos(k\pi h)\right)^n\right| \\ &= \frac{1}{5^n}\left(\max_k\left|1-2\cos(k\pi h)\right|\right)^n \\ &= \frac{1}{5^n}\left(1+2\cos(\pi h)\right)^n\end{aligned}$$

3.4.3 Influence of the mesh size

For both problems the spectral radius of one iteration depends on the mesh size h. It is interesting to see how the iteration behaves when the mesh size tends towards 0. When $h \to 0$ we have $\cos(\pi h) \to 1$. Hence,

the spectral radius of each problem has the following property

$$\rho(G_n^A) \to \frac{1}{3^n}(1+2)^n = 1$$

which means that no matter how n is big, the method tends to a non-convergent one, whereas

$$\rho(G_n^B) \to \left(\frac{3}{5}\right)^n$$

which means that even in the worst case, the method will be convergent in a reasonable time for the shape optimization problem. We have already explained this main difference in the previous sections. Indeed, the shape optimization problem as stated here is not a stiff problem. This is however not always the case for all parameterizations or when physics comes into consideration.

In the next section our aim is to show how we can improve this convergence result with a MG strategy. By improving we mean to find an ideal MG cycle whose convergence rate will be smaller and mesh independent.

4 Multigrid methods for parametric shape optimization

The popularity of MG methods relies on two properties: (1) the convergence rate is mesh size independent; (2) the computational work is proportional to the number of nodes N.

Let us sketch here briefly the basic ideas of the MG methods (we refer to [25] for a complete review). Assume that you are given a mesh, namely the fine mesh. The approximation space defined on this mesh can be seen as the direct sum of two complementary subspaces: a low frequency space and a high frequency space. The efficiency of MG methods for solving a PDE relies on the complementarity of two "ingredients":

1. a simple iterative method (Jacobi, Gauss-Seidel, SOR, etc.) reduces easily the high frequency components of the error: the *smoother* or *solution operator*;
2. transfer operators between the fine mesh and coarser meshes are used to reduce or annihilate the remaining low frequency part of the error (Coarse Grid Correction).

MG cycles are composed of relaxation phases (smoothing phases) and Coarse Grid Corrections via transfer operators. On the unique fine grid we have seen that the spectral radius of the solution operator is mesh size dependent and close to 1 (a bad convergence rate on the LF subspace). In the MG strategy, the smoother is such that the convergence rate on the HF subspace is mesh size independent. Then the LF modes are well represented (if not exactly) on a coarser mesh. Relatively to this coarse mesh, the modes of highest frequency within the LF modes become the HF modes. Again, the solution operator can be used on this new mesh to reduce efficiently (*i.e.* at a mesh size independent convergence rate) the error in the newly defined HF subspace. Moreover the computational work is smaller on this coarser mesh. This can be repeated recursively on coarser meshes. On the coarsest mesh, the number of d.o.f. is assumed to be small enough to be able to solve the problem exactly (for instance with a direct method). In that case the MG algorithm is said to be *ideal*.

A MG cycle can be seen as a linear iteration. Rigorously, we need to investigate the spectrum of the amplification matrix of one MG cycle. An ideal two-level cycle is sufficient to prove that the convergence is mesh size independent or not. This is the aim of this section. If we are mainly interested in the shape optimization problem, we will nevertheless recall the proof for the Poisson equation.

The Poisson equation is the typical problem for linear MG. Indeed, the eigenstructure of the discrete problem is such that the transfer to the coarse grid is exact (discrete Fourier modes); in 1D, the Jacobi method is a good smoother for the upper half of the spectrum (mesh size independent). In the framework of shape optimization problems, these properties are not straightforward. In the special case of the L_2 best approximation in a space of piecewise linear functions, the transfer between grids is also exact (the eigenvectors are the same discrete Fourier modes). Unfortunately the decay factors of a simple method

(Jacobi/gradient) do not have the required smoothing property. On the contrary we have seen that the LF components are better decayed: the solution operator is an *anti-smoother*. Hence one may argue that a MG would be suitable. Obviously the restriction to a coarser grid would not be necessary since the problem would already have been solved on this subspace. Let us show this rigorously by studying the convergence of an ideal cycle. Later, we will suggest alternative transfer operators for shape optimization problems for which we conduct similar convergence analysis of ideal cycles.

4.1 Transfer operators

Let us consider two grids $\mathcal{T}_h$ and $\mathcal{T}_{2h}$ as defined in section 2.1.3 with respectively N and N' interior nodes (see Figure 6). They are referred as the fine grid and the coarse grid. Assume that the problem dimensions are $N = 2^p - 1$ on the fine grid and $N' = 2^{p-1} - 1$ on the coarse grid for some $p > 1$. In that case the relation $2N' + 1 = N$ holds, which is equivalent to say that the interval on the coarse grid h' is twice bigger $h' = 2h$.

We first need to define transfer operators between these grids, a prolongation operator $P : \mathcal{T}_{2h} \to \mathcal{T}_h$ and a restriction operator $R : \mathcal{T}_h \to \mathcal{T}_{2h}$. Since we have assumed Dirichlet boundary conditions, we only need to define transfer operators between the interior nodes.

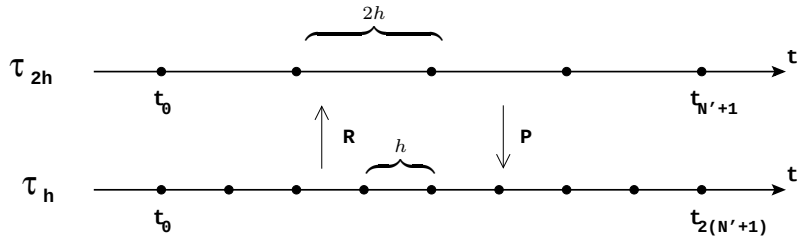

Figure 6: fine $\mathcal{T}_h$ and coarse $\mathcal{T}_{2h}$ discretizations

Once these operators are defined, two definitions of a coarse subproblem are distinguished (see [25]):

- Galerkin Coarse grid Approximation (GCA): the matrix of the coarse problem A' is obtained by projection of the matrix of the fine problem using the transfer operators, *i.e.* $A' = RA_hP$;
- Discrete Coarse grid Approximation (DCA): the matrix of the coarse problem A' is obtained by discretization on the mesh $\mathcal{T}_{2h}$ of the original problem, *i.e.* $A' = A_{2h}$.

If the transfer operators are well defined, both definitions may be equivalent. This property is not compulsory but convenient for convergence proofs[3].

In the sequel we define P as the linear interpolation operator:

$$P = \begin{pmatrix} \frac{1}{2} & & & & & & \\ 1 & & & & & & \\ \frac{1}{2} & \frac{1}{2} & & & & & \\ & 1 & & & & & \\ & \frac{1}{2} & & & & & \\ & & \ddots & & & & \\ & & & \frac{1}{2} & & & \\ & & & 1 & & & \\ & & & \frac{1}{2} & \frac{1}{2} & & \\ & & & & 1 & & \\ & & & & \frac{1}{2} & & \end{pmatrix}. \tag{32}$$

[3]These properties, $A_{2h} = RA_hP$ and $\alpha > 0$ such that $R = \alpha P^T$, are known as the *variational properties*.

Regarding the Poisson equation, if the restriction operator is the mean operator $R = \frac{1}{2}P^T$, then both definitions GCA and DCA are equivalent ($A_{2h} = \frac{1}{2}P^T A_h P$). Regarding the shape optimization problem, the equivalence is achieved with $R = P^T$ ($H_{2h} = P^T H_h P$).

In the sequel, we illustrate the multilevel scheme with the following notations: $\searrow$ is the restriction operator, $\nearrow$ or $\uparrow$ the prolongation operator, $\square$ a relaxation phase and $\blacksquare$ an ideal correction. Let $r_h = A_h u_h - f_h$ (resp. $r_h = H_h x - b_h$) be the residual. By linearity, for all u_h (resp. x) we have the equality $Ae_h = Au_h - f_h = r$ (resp. $H_h e_h = H_h x - b_h = r_h$) where u^* (resp. x^*) is the exact solution and $e_h = u_h - u^*$ (resp. $e_h = x - x^*$) the error.

4.2 Two-grid ideal algorithms

The optimal multilevel algorithm is the FMG algorithm: it is a combination of *Nested Iteration* and V-cycles (or saw-tooth, W-cycles). The overall efficiency of this algorithm relies on the efficiency of one cycle; in that sense the two-grid ideal algorithm is the reference algorithm since at any lower grid, one can use recursively an other cycle. This is sufficient for proof and therefore we restrict ourselves to this case. For more details we refer the reader to [25].

We want to solve the linear systems $A_h u_h = f_h$ and $H_h x = b_h$ on the fine grid $\mathcal{T}_h$. The following algorithms are said to be ideal in the sense that the CGC is done exactly.

Remark 5. *In the sequel, the context of the problem will be obvious (Poisson equation or shape optimization). Therefore we skip the superscripts ^{A} and ^{B} for the sake of simplicity.*

4.2.1 Classical formulation

Let $\mathcal{T}_h$ and $\mathcal{T}_{2h}$ be two grids as defined in the section 2.1.3. The initial approximation is noted $u_h^{(0)}$. A two-grid ideal algorithm involves three phases:

1. a pre-relaxation phase on the fine grid: the error is smoothed with a few Jacobi iterations; an other approximation $u_h^{(1)}$ is obtained:
$$u_h^{(1)} = G_k u_h^{(0)} + f_h' \tag{33}$$
2. a coarse grid correction phase: the residual
$$r = A_h u_h^{(1)} - f_h \tag{34}$$
verifies the following equation on the coarse grid
$$RA_h P e_{2h} = Rr \tag{35}$$
which is solved exactly. We deduce a second approximation of the solution on the fine grid by prolongation of the error e_{2h} as a correction term
$$u_h^{(2)} = u_h^{(1)} - Pe_{2h} = u_h^{(1)} - P\left(RA_h P\right)^{-1} Rr \tag{36}$$
3. a post-relaxation phase: the final approximation is given with relaxation of $u_h^{(2)}$, that is
$$u_h^{(3)} = G_k u_h^{(2)} + f_h' \tag{37}$$

These three phases are illustrated on the Figure 7.

For the convergence analysis of such an algorithm, it is sufficient to consider a single Jacobi iteration as relaxation phase w.l.o.g., (see Algorithm 1). The amplification matrix equivalent to the ideal cycle reads
$$G = G_\tau \left[I - P\left(RA_h P\right)^{-1} RA_h\right] G_\tau. \tag{38}$$

The efficiency of this ideal cycle is proved using the spectral decomposition of G.

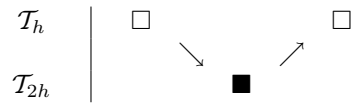

Figure 7: Two-grid ideal algorithm (V-cycle)

Algorithm 1: MG ideal V-cycle

`Relaxation`

$$u_h^{(1)} = G_\tau u_h^{(0)} + f_h'$$

`Coarse Grid Correction`

$$r = A_h u_h^{(1)} - f_h$$

$$RA_h P e_{2h} = Rr$$

$$u_h^{(2)} = u_h^{(1)} - P e_{2h} = u_h^{(1)} - P\left(RA_h P\right)^{-1} Rr$$

`Relaxation`

$$u_h^{(3)} = G_\tau u_h^{(2)} + f_h''$$

4.2.2 Spectral radius of the ideal cycle

The convergence proof is given in the Appendix A.2 for a sake of comparison with the shape optimization problem. Here is a sketch of the proof: first we show that G is similar to a matrix of the form ΣD^2. We deduce the spectrum of G according to the one of ΣD^2. We have the following:

- there are N' eigenvalues equal to zero;
- there are $N'+1$ eigenvalues equal to $\frac{1}{9}$;

thus $\rho(G) = \frac{1}{9}$. In short, the method converges ($\rho < 1$) and the convergent rate is mesh-independent. This result shows the optimal efficiency of the MG method.

To fix an idea, if the fine grid is such that $N = 31$ ($h = \frac{1}{32}$) we can compute the number of Jacobi iterations needed to reach the same convergence rate. That is, we look for the number of iterations n such that

$$\rho(G_n) \leq \frac{1}{9} \tag{39}$$

which is

$$n \geq \frac{\log(9)}{\log(3) - \log(1 + 2\cos\pi h)} \approx 684 \tag{40}$$

Given that we have considered two Jacobi iterations as pre- and post-relaxation phases, we need the computational work done for the CGC to be less that 682 iterations. For complexity results we refer to [7, 25].

4.2.3 Optimization formulation

We are now interested in the shape optimization problem. First we apply "mechanically" the two-grid scheme as described in section 4.2.1. We still consider the P1 parameterization on $\mathcal{T}_h$ and T_{2h} as well as the linear interpolation operator P as prolongation operator.

Let us sketch a similar ideal algorithm in the framework of the shape optimization problem. Let $x^{(0)}$ be an initial approximation of the optimal design parameters. Let us describe the different phases of an ideal algorithm in the optimization terminology:

- The relaxation phase is regarded as one steepest descent iteration on the scaled problem with step τ;
- In term of optimization, the CGC is still an optimization problem. Hence the ideal CGC returns the minimum of the objective on the coarse mesh:

$$\min_{y \in \mathcal{T}_{2h}} J(x + Py) \tag{41}$$

for a given x obtained for instance by a previous relaxation. The objective function on the coarse grid remains quadratic and the domain is convex, hence the global minimum is fully characterized by its stationary conditions.

With a pre-relaxation phase and a post-relaxation phase we have the Algorithm 2.

Algorithm 2: Optimization MG ideal V-cycle

`Relaxation`

$$x^{(1)} = G_\tau x^{(0)} + b'_h$$

`Coarse Grid Correction`

$$\Delta y = \arg\min_{y \in \mathcal{T}_{2h}} j(y) = J(x^{(1)} + Py)$$

$$x^{(2)} = x^{(1)} + P\Delta y$$

`Relaxation`

$$x^{(3)} = G_\tau x^{(2)} + b''_h$$

When the objective is strictly convex and without constraints, the minimum is uniquely characterized by the stationary conditions. Let us introduce the stationary conditions in the CGC. Since the gradient is linear we have

$$\begin{aligned} g(y) &= P^T J'(x^{(1)} + Py) \\ &= P^T (H_h(x^{(1)} + Py) - b_h) \\ &= P^T H_h P y + P^T (H_h x^{(1)} - b_h) \\ &= P^T H_h P y + P^T r \end{aligned}$$

where $r = H_h x^{(1)} - b_h$ is the residual. The stationary conditions on the coarse grid read $g(\Delta y) = 0$:

$$\Delta y = -\left(P^T H_h P\right)^{-1} P^T r \tag{42}$$

hence

$$x^{(2)} = x^{(1)} - P\left(P^T H_h P\right)^{-1} P^T r. \tag{43}$$

Therefore the amplification matrix equivalent to the cycle reads

$$G = G_\tau \left[I - P\left(P^T H_h P\right)^{-1} P^T H_h\right] G_\tau \tag{44}$$

which has exactly the same structure as the amplification matrix (38). Note that the restriction operator must be the transpose of the prolongation operator:

$$R = P^T. \tag{45}$$

4.2.4 Spectral radius of the ideal cycle

The details of the convergence proof is given in the appendix section A.3. As for the Poisson equation we first apply similar transformations to simplify the diagonalization. We show that G is also similar to a matrix of the form ΣD^2 where D is diagonal and Σ's structure illustrate in the Figure 34.

The eigenvalues are however more difficult to derive. Indeed, if the Σ structure is simple, it is harder to simplify its entries. We adopt the following strategy:

a) an ansatz on the eigenvectors structure (non-zero entries) is set;

b) linear systems are deduced from this hypothesis;

c) these linear systems are solved using the symbolic calculus software Maple©;

d) the solutions and their linear independence are verified.

In short, we obtain the following results:

- there are n' eigenvalues α_k equal to zero;
- $\alpha_{n'+1} = \frac{1}{25}$ is an obvious eigenvalue;
- the remaining n' eigenvalues given by Maple are

$$\alpha_{n'+1+k} = \frac{1}{25}\frac{27 - 144\cos^2\left(\frac{\theta_k}{2}\right) + 304\cos^4\left(\frac{\theta_k}{2}\right) - 320\cos^6\left(\frac{\theta_k}{2}\right) + 160\cos^8\left(\frac{\theta_k}{2}\right)}{3 - 8\cos^2\left(\frac{\theta_k}{2}\right) + 8\cos^4\left(\frac{\theta_k}{2}\right)}.$$

Hence the spectral radius of the ideal cycle is

$$\begin{aligned}\rho(\Sigma D^2) &= \max_{k=1..n} |\alpha_k| \\ &= \max_{k=n'+1..n} |\alpha_k|\end{aligned}$$

At this stage one can show that $\alpha_{n'+1+k} > \frac{1}{25}$ for $k = 1 \ldots n'$ and that α is a monotonous decreasing function on the interval $\theta \in]0\ \frac{\pi}{2}[$. Thus the maximum is attained at $\theta = \theta_1$, *i.e.* $\rho(\Sigma D^2) = \alpha_{n'+2}$, which is mesh-dependant. When the meshsize tends to zero ($h \to 0$) we have $\alpha_{n'+2} \to \frac{9}{25} = (\frac{3}{5})^2$. This is exactly the convergence rate of 2 Jacobi iterations (see section 3.4). In other words, the Coarse Grid Correction is useless.

4.3 Alternative transfer operators for shape optimization

We have previously seen that the classical strategy fails in the case of the optimization problem. The reason is that we lack the complementarity between the fine grid and the coarse grid: the relaxation phase behaves as a *anti-smoother* while the restriction operator on the coarse grid still behaves as a low-pass filter, the only modes whose error have already been well damped, *i.e.* the LF modes, can be represented. The zero eigenvalues of the amplification matrix corresponds to the annihilated modes: the LF modes.

In this section we focus on the definition of new transfer operators for shape optimization. In this framework, the concepts of prolongation and restriction are extended to any kind of parameterizations such as Bézier curves, B-splines, etc., which are defined continuously on the domain, although the analysis is still done with the P1 CAD-free formulation. In addition, we guarantee that the new definition is consistent with the previously defined transfer operators between meshes (discrete structures).

Let F be the reference search space (the fine "grid") and V a subspace of F (the coarse "grid"). F is isomorphic to $\mathbb{R}^N$ and V to $\mathbb{R}^{N'}$ ($N' < N$). As seen in the section 2.1.2, the fine space relies on the basis $\{u_k\}_{k=1}^N$ (the so-called parameterization). As element of the fine space, any element v of $V \subset F$ can be written in this basis. In a general abstract formulation, a subspace V is defined by

$$V \equiv \left\{ v = \sum_{k=1}^{N} x_k u_k \in F \quad \middle| \quad x = Qy, \quad \forall y \in \mathbb{R}^{N'} \right\} \tag{46}$$

where Q is the matrix of the linear application from $\mathbb{R}^{N'}$ to $\mathbb{R}^N$ that maps the components of v in V to the parameterization basis F (the columns of Q are a basis of V in F): it can be seen as a prolongation operator.

The subspaces V are regarded as correction spaces. In other words, for a given $x^* \in F$, the coarse problem is a minimization problem on the affine subspace $x^* + V$, *i.e.* $x = x^* + \Delta x$ where $\Delta x = Qy$ for some $y \in \mathbb{R}^{N'}$. Thus the parametric objective function of the coarse problem reads

$$j(y) = J(x^* + Qy). \tag{47}$$

The gradient of j reads

$$g(y) = Q^T G(x^* + Qy) \tag{48}$$

and its Hessian

$$h(y) = Q^T H(x^* + Qy)Q. \tag{49}$$

The CGC (ideal by complete resolution) of the Algorithm 2 can be rewritten as

$$\Delta y = \arg\min_{y \in V} j(y) = J(x^{(1)} + Qy)$$

$$x^{(2)} = x^{(1)} + Q\Delta y$$

The amplification matrix equivalent to this new cycle reads

$$G = G_\tau \left[I - Q \left(Q^T H_h Q \right)^{-1} Q^T H_h \right] G_\tau. \tag{50}$$

Note that the restriction operator is automatically taken as the transpose of the prolongation operator. We do not know anything about $Q^T H_h Q$ *a priori*. Hence the coarse subproblem is defined in the sense of a GCA. In other words the choice of the transfer operator Q defines the sense of the "coarse grid". Here, coarse means fewer degrees of freedom but not necessarily a smoother approximation. This definition is consistent with the previous definition when Q is appropriately chosen. Three cases are considered:

1. the subspaces are embedded parameterizations (called Y method);
2. the subspaces are embedded parameterizations preconditioned by a perdiagonal permutation matrix (called Z method) (as suggested in [8]);
3. the subspaces are eigenspaces (called Ω method).

For each of these cases the spectral radius of the ideal cycle is examined when the fine parameterization is composed of P1 elements.

4.3.1 Embedded parameterizations

Assume that we are provided with embedded parameterization spaces $V_1 \subset V_2 \subset \cdots \subset V_N$. Each of it is considered with a basis $\{u\}_{k=1}^{N'}$ (*e.g.* polynomial spaces of increasing degree and Bernstein basis, B-splines of constant degree/order and increasing number of splines with knots insertion, etc.). Let $F = V_N$. We assume that for any of these spaces there exists a linear application from $\mathbb{R}^{N'}$ to $\mathbb{R}^N$ noted $E^N_{N'}$ such that

$$\forall y \in \mathbb{R}^{N'}, \quad x = E^N_{N'} y \quad \Longrightarrow \quad v = \sum_{k=1}^{N'} y_k u_k^{N'} = \sum_{k=1}^{N} x_k u_k^N \in V_{N'}. \tag{51}$$

In other words $E^N_{N'}$ is the application that maps the components of v in $V_{N'}$ in the basis of F. For polynomial spaces $\mathcal{P}^{N'}$ and $\mathcal{P}^N$ (of dimension $N'+1$ and $N+1$ resp.) in the Bernstein basis this application results from the so-called *degree elevation* property [10]. Formally the subspaces read

$$V_{N'} \equiv span\{u_k^{N'}\} \equiv \left\{ v = \sum_{k=1}^{N} x_k u_k^n \in F \;\middle|\; x = E^N_{N'} y, \quad \forall y \in \mathbb{R}^{N'} \right\} \iff Q = E^N_{N'}. \tag{52}$$

Remark 6. *The prolongation operator $Q = E^N_{N'}$ shows a trivial structure when the basis of the subspaces V'_N are composed of subsets of the fine space basis F. This is the case of the canonical basis and orthogonal polynomials for polynomials spaces. Precisely, this operator reads*

$$E^N_{N'} = \begin{pmatrix} I_{N'\times N'} \\ 0_{(N-N')\times N} \end{pmatrix}.$$

If the parameterization space is defined with P1 elements, then Q is the classical linear interpolation operator $Q = P$. We have shown that in that case the algorithm is not efficient because a gradient iteration behaves as an anti-smoother operator. For other parameterization, such as the Bézier parameterization, numerical experiments corroborate this result [26, 5].

4.3.2 Preconditioning by spectrum permutation

In this second section we examine the method proposed in [8]. We keep the assumption under which we are provided with embedded parameterizations and their basis together with the classical prolongation operators $E^N_{N'}$. We will use the fact that high frequency modes converge slowly. A new transfer operator is designed such that high frequency modes are projected on a "coarse grid".

Let H be the Hessian matrix. It is a real s.p.d. matrix, therefore diagonalizable with orthogonal eigenvectors and real positive eigenvalues: $H = \Omega\Lambda\Omega^T$, $\Omega^T\Omega = \Omega\Omega^T = I_N$. We suppose (w.l.o.g.) that the eigenvalues λ_k are ordered increasingly. Let us consider the following subspaces:

$$V_{N'} \equiv \left\{ v = \sum_{k=1}^{N} x_k u_k \in F \quad \middle| \quad x = \Omega\mathbb{P}\Omega^T E^N_{N'} y, \quad \forall y \in \mathbb{R}^{N'} \right\} \iff Q = \Omega\mathbb{P}\Omega^T E^N_{N'} \tag{53}$$

where $\mathbb{P}$ is the perdiagonal permutation matrix

$$\mathbb{P} = \begin{pmatrix} & & 1 \\ & \iddots & \\ 1 & & \end{pmatrix}. \tag{54}$$

The role of such a transfer operator is to reorganize the eigenpairs such that the relaxation operator becomes a smoother (in the search space, *i.e.* for the variable y, but an anti-smoother for the shape).

4.3.3 Spectral radius of the ideal cycle

We still consider the P1 parameterization on each level and $E^n_{n'} = P$. We conduct a spectral analysis of the amplification matrix (50) with $Q = \Omega\mathbb{P}\Omega^T P$. We adopt the same methodology used to derive the spectral radius of the classical method:

a) the coarse grid problem (GCA) $H' = Q^T H_h Q$ is simplified;

b) we deduce a simpler form for $I - QH'^{-1}Q^T H_h$ and similar transformations are applied to G; it follows that G is again similar to a matrix of the form ΣD^2 where D is diagonal;

c) the entries of Σ exhibit a structure illustrated in the Figure 34;

d) an ansatz is proposed for the eigenvector structure of ΣD^2 and the linear systems are solved using Maple. An analytical formula is obtained, providing the spectral radius.

The proof is done in section A.4. We find $\rho(G) = \frac{1}{25}$.

4.3.4 Eigenspace transfer operator

In this last method the embedded parameterizations are not necessary. It can be seen as an algebraic version of the MG algorithm. Let us consider a single fine space F with the basis $\{u_k\}$. Subspaces are directly deduced from the Hessian diagonalization: the subspace of dimension N' is the space spanned by the last N' eigenvectors (we have assumed that the eigenvectors are decreasingly ordered to be consistent with section 2.3), *i.e.*

$$H = \Omega\Lambda\Omega^T = \begin{pmatrix}\Omega_1 & \Omega_2\end{pmatrix}\begin{pmatrix}\Lambda_1 & 0\\ 0 & \Lambda_2\end{pmatrix}\begin{pmatrix}\Omega_1^T\\ \Omega_2^T\end{pmatrix} \tag{55}$$

where

$$\Omega_1 = \begin{pmatrix}\omega_1 & \dots & \omega_{N-N'}\end{pmatrix}, \quad \Omega_2 = \begin{pmatrix}\omega_{N+1-N'} & \dots & \omega_N\end{pmatrix} \tag{56}$$

and

$$V_{N'} \equiv span\{\Omega_2\} \equiv \left\{ v = \sum_{k=1}^{N} x_k u_k \in F \;\middle|\; x = \Omega_2 y,\ \forall y \in \mathbb{R}^{N'} \right\} \iff Q = \Omega_2. \tag{57}$$

The parametric Hessian reads

$$h = \Omega_2^T H \Omega_2 = \Lambda_2 \tag{58}$$

whose conditioning is necessarily better than the fine space Hessian since

$$\kappa_2(h) = \frac{\lambda_{N+1-N'}}{\lambda_N} < \frac{\lambda_1}{\lambda_N} = \kappa_2(H). \tag{59}$$

Remark 7. *One may consider linear equality constraints. In such case H is taken as the projected Hessian. The eigenvectors Ω belong to the feasible space. A coarse correction is transferred to the feasible "fine grid" using the orthonormal basis Z of the kernel of the constraints: $x = Z\Omega_2 y$ and $Q = Z\Omega_2$. Thus the coarse search spaces are not submitted to any additional constraints.*

4.3.5 Spectral radius of the ideal cycle

The proof is much simpler than for the previous method, using the fact that the coarse grid basis is exactly composed of eigenvectors. Thanks to orthogonality properties, G is straightforwardly simplified. We deduce that $\rho(G) = \frac{1}{25}$ (see section A.5).

4.3.6 Comparison of the ideal algorithms with a single-level method

After permutation or eigenspace correction, the spectral radius of an ideal cycle is independent of the mesh size. With two Jacobi/gradient iterations (pre- and/or post-relaxation) with step $\tau = \frac{4}{5}$ this radius is

$$\rho_{MG} = \frac{1}{25}. \tag{60}$$

A n-steps Jacobi/gradient method would give (see 3.4)

$$\rho_J < \left(\frac{3}{5}\right)^n \tag{61}$$

for all mesh size. Hence we would only need $n \geq \frac{\log(25)}{\log(5)-\log(3)} \approx 6.30$ iterations to reach the same convergence rate (*i.e.* $n \geq 7$).

In other words, the work done on the coarse grid should not excess the work done to run 5 Jacobi iterations for the MG algorithm to be more efficient. Again, this is due to the fact that the shape optimization problem is well conditioned with P1 elements. The conditioning might however become drastically bad with other parameterizations (*e.g.* Bernstein polynomial, Bézier representation) or when physics comes into consideration.

4.4 Numerical experiments

In order to illustrate and confirm the theoretical results, let us realize numerical experiments of the two-grid algorithms. The parameterization is piecewise linear (P1) on the grids $\mathcal{T}_{2^p h}$ where $p = 0, 1, 2, \ldots$ and $h = \frac{1}{N+1}$ is the meshsize of the finest grid. The RHS is given by the shape illustrated in the Figure 8. This experience is realized for $N = 256$ and $N = 1024$.

The convergence is represented in terms of the discrete L_2 norm of the residual $r(x) \stackrel{\text{def.}}{=} \|H_h x - b_h\|_{L_2}$. The threshold is set to $\varepsilon = 10^{-14} \cdot r^0$ where $r^0 = r(x^{(0)})$ is the residual of the initial approximation $x^{(0)} = \mathbf{0}$.

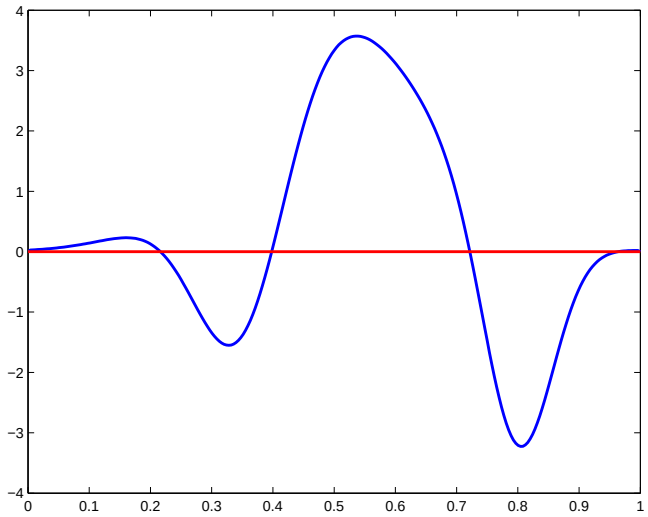

Figure 8: target shape (blue) and initial approximation (red)

4.4.1 Parameterization $N = 256$

Algorithm settings:

- levels: $p = 0, \ldots, 7$
- relaxation parameter: $\tau = \frac{4}{5}$
- pre-relaxation: $\nu_1 = 1$ Jacobi iteration
- post-relaxation: $\nu_2 = 1$ Jacobi iteration

The results are illustrated in the Figures 9 (Jacobi), 10 (classical MGV), and 11 (optimization MGV). As expected, the convergence rate of the Jacobi method tends to $\frac{3}{5} = 0.6$. The threshold is reached after 40 iterations. The main components of the residual are HF modes. The convergence rate of the classical MGV method tends to $(\frac{3}{5})^2 = 0.36$, that is, the convergence rate equivalent to 2 Jacobi iterations (1 pre- and 1 post-relaxation). The threshold is reached after about 24 cycles (equivalent to 48 Jacobi iterations on the fine grid). The main components of the residual are still HF modes. Finally, the computed convergence rate of the optimization MGV method is equal to $\frac{1}{25} = 0.04$ as expected. The convergence is reached after 11 cycles (equivalent to 22 Jacobi iterations on the fine grid). The main components of the residual are LF modes.

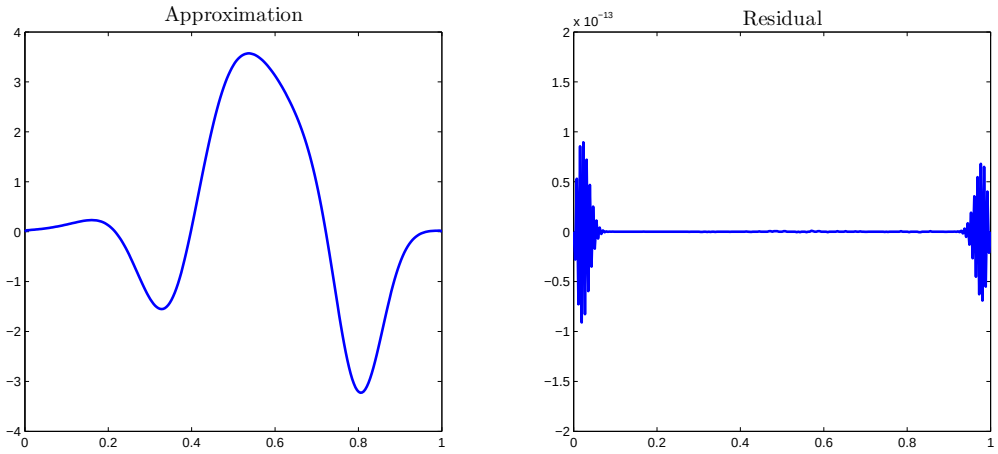

(a) Approximation and residual

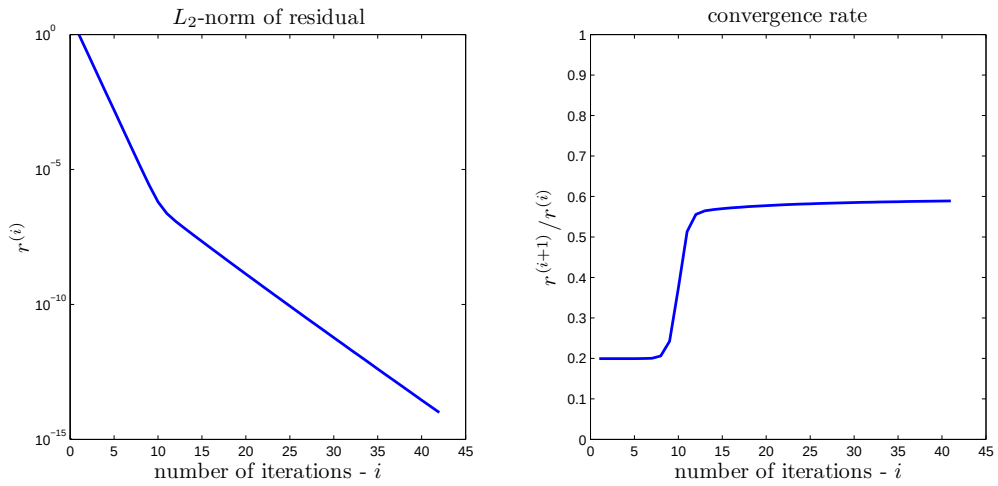

(b) Convergence and convergence rate

Figure 9: Jacobi method, $N = 256$

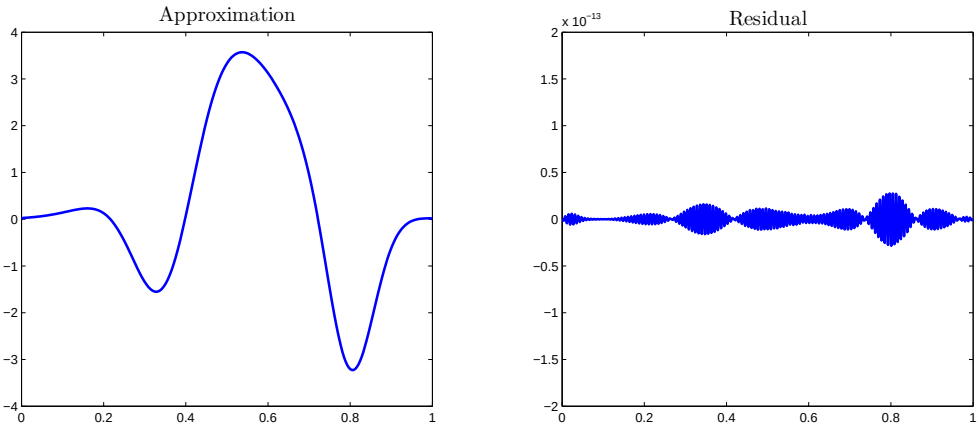

(a) Approximation and residual

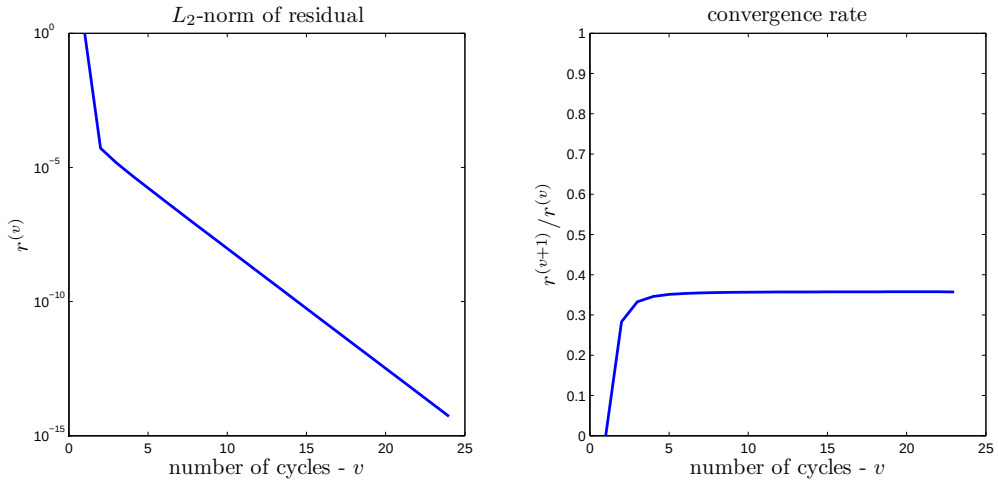

(b) Convergence and convergence rate

Figure 10: classical MGV method, $N = 256$

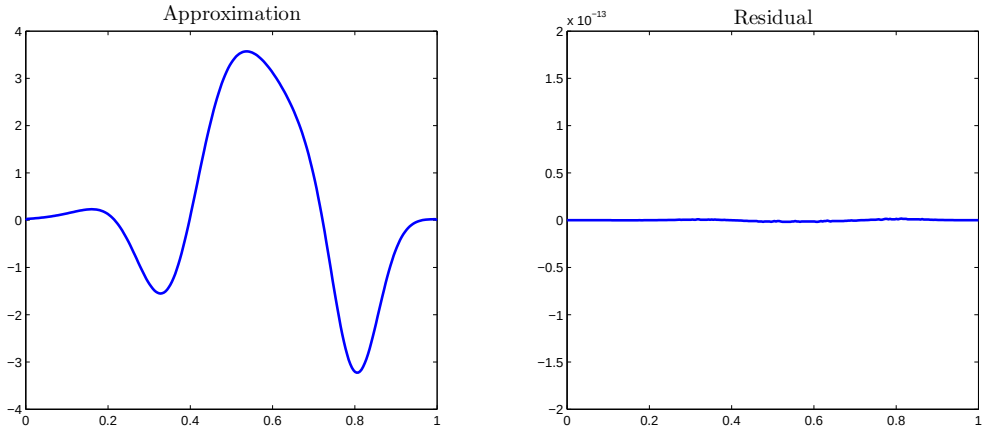

(a) Approximation and residual

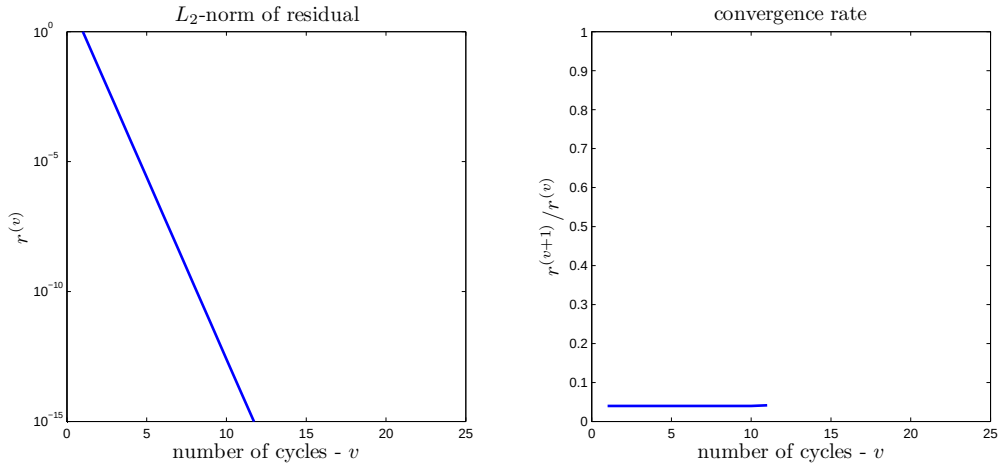

(b) Convergence and convergence rate

Figure 11: optimization MGV method, $N = 256$

4.4.2 Parameterization $N = 1024$

Algorithm settings:

- levels: $p = 0, \ldots, 9$
- relaxation parameter: $\tau = \frac{4}{5}$
- pre-relaxation: $\nu_1 = 1$ Jacobi iteration
- post-relaxation: $\nu_2 = 1$ Jacobi iteration

The results are illustrated on the Figures 12 (Jacobi), 13 (classical MGV), and 14 (optimization MGV). For the three methods, the convergence rates are identical to those of the previous experiences with $N = 256$. Consequently, the same number of cycles is needed to reach the convergence threshold.

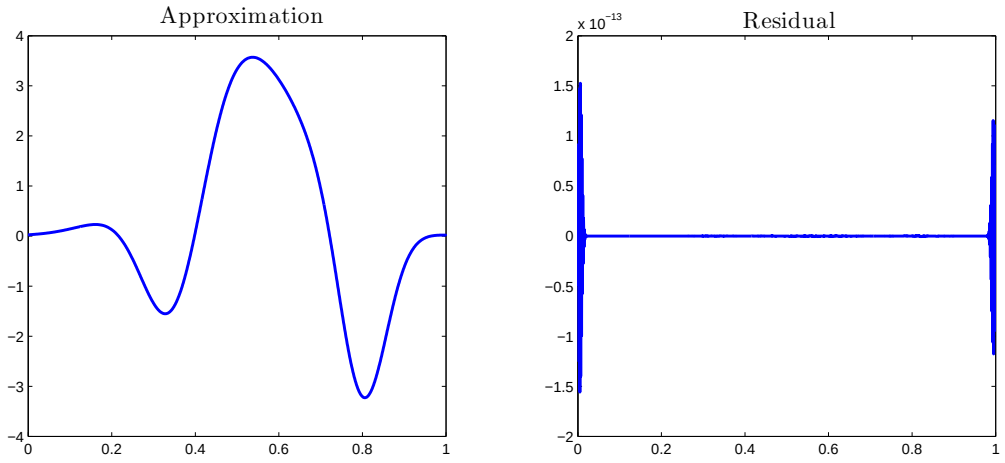

(a) Approximation and residual

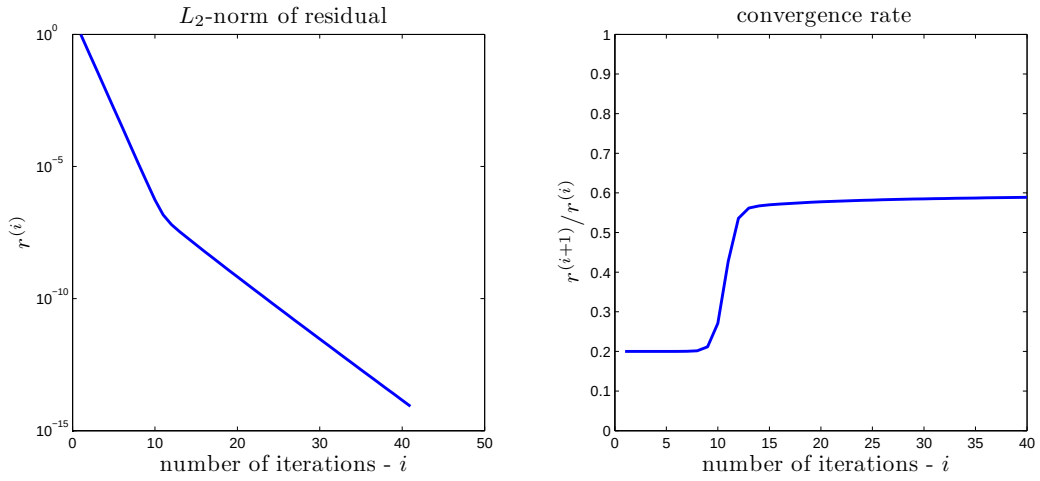

(b) Convergence and convergence rate

Figure 12: Jacobi method, $N = 1024$

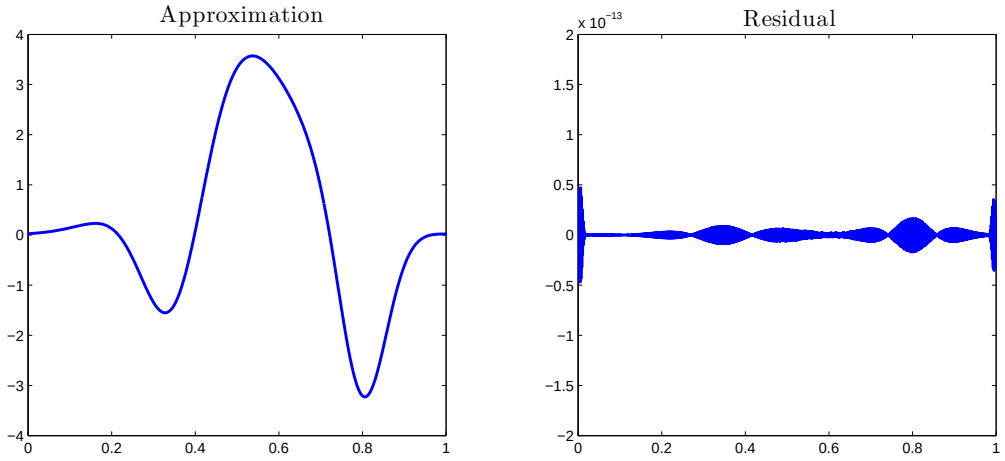

(a) Approximation and residual

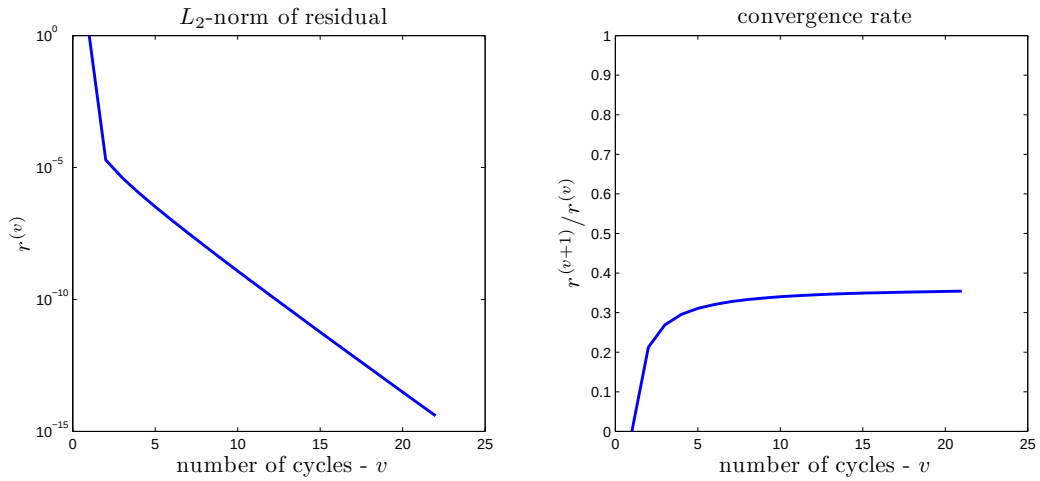

(b) Convergence and convergence rate

Figure 13: classical MGV method, $N = 1024$

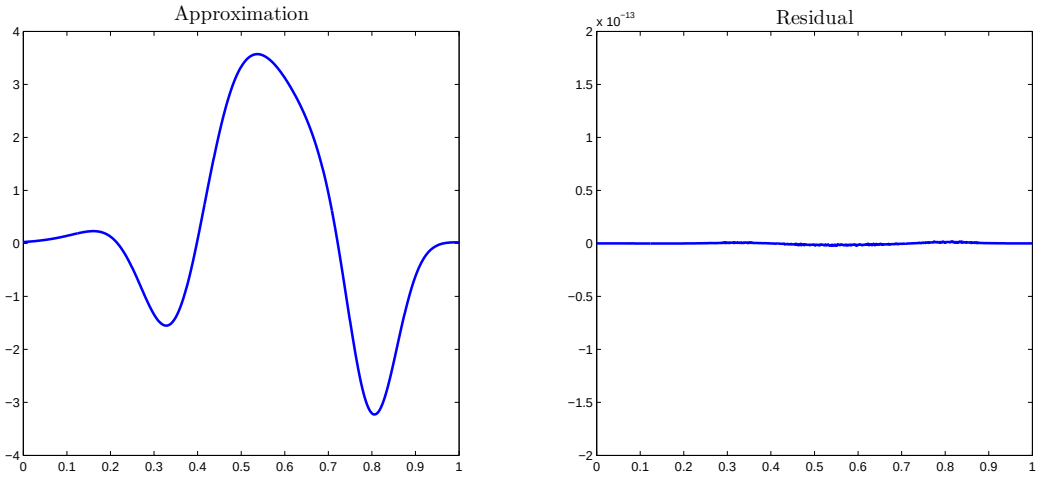

(a) Approximation and residual

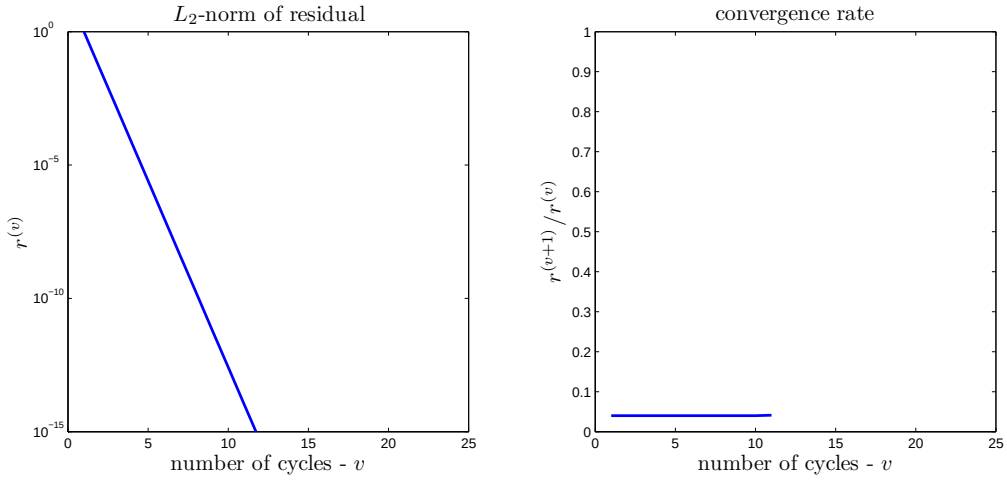

(b) Convergence and convergence rate

Figure 14: optimization MGV method, $N = 1024$

5 Stiffness due to the parameterization

The stiffness of the optimization problem is closely related to the bad or ill conditioning of the Hessian matrix. Let us compute the condition number of the Hessian matrix for different parametric basis functions and w.r.t. the space dimension. Before that, let us recall that the matrix norm induced by the vector norm $\|\cdot\|_p$ is defined by

$$\|A\|_p = \sup_{x \neq 0} \frac{\|Ax\|_p}{\|x\|_p}. \tag{62}$$

The condition number κ_p w.r.t. the norm $\|\|_p$ of an invertible A is

$$\kappa_p(A) = \|A\|_p \left\|A^{-1}\right\|_p. \tag{63}$$

In particular, for $p = 2$ we have

$$\kappa_2(A) = \frac{\lambda_n}{\lambda_1}. \tag{64}$$

5.1 Bézier parameterization

The best approximation problem can be formulated in a polynomial space. Using a Bézier representation of the graph of u consists in using the Bernstein polynomials as basis functions. Compared to the class of piecewise linear shapes, a smooth shape is obtained with few parameters.

The Bernstein polynomials are defined on $[0\ 1]$ by

$$B_N^k(t) = C_N^k t^k (1-t)^{N-k} \tag{65}$$

where $C_N^k = \frac{N!}{k!(N-k)!}$ are the binomials coefficients. We initially define $N+2$ basis functions u_k by $u_k = B_{N+1}^k$. Since only B_0^{N+1} in non-zero at $t = 0$ and B_{N+1}^{N+1} non-zero at $t = 1$, the Dirichlet boundary conditions read merely

$$x_0 = 0 \qquad \text{and} \qquad x_{N+1} = 0.$$

Hence the projected Hessian on the feasible space is straightforwardly obtained by removing the first and the last lines and columns of the Hessian matrix. The elements of the Hessian matrix are given by [10]

$$h_{kj} = \int_0^1 u_k(t) u_j(t) dt = \frac{C_{N+1}^k C_{N+1}^j}{C_{2(N+1)}^{k+j}} \frac{1}{2(N+1)+1}. \tag{66}$$

We do not know any closed form for the eigenpairs of such a matrix, but we can compute them numerically.

To be consistent with the analysis conducted with the piecewise linear elements, we assume that the problem has been scaled beforehand (that is, preconditioned by the inverse of the diagonal of the Hessian matrix). In that form the steepest descent method is equivalent to the Jacobi iterations. To investigate the decay factors we must compute the eigenpairs of $D_H^{-1}H$ where D_H is the diagonal part of H, the projected Hessian. The Figures 15 and 16 depict the eigenvectors and the eigenvalues respectively.

A spectral structure similar to the one obtained with the P1 elements can be observed: the eigenvectors are Fourier-like modes; the LF modes are associated to the largest eigenvalues and the HF modes to the smallest. The main difference is that the matrix is ill-conditioned: with $N = 16$ we have $\kappa_2(D_H^{-1}H) \approx 10^9$. This yield an amplification matrix for which no τ can be set to define a smoother. In order to illustrate that H amplifies the LF modes let us look at the Krylov vectors q^i for some random vector x_0 and $N = 32$ depicted in the Figure 17.

Finally, the Figure 18 shows the decay function of one descent iteration for which the amplification matrix reads

$$G_\tau = I - \tau D_H^{-1} H.$$

The convergence is obtained iff $\tau \in]0\ \frac{2}{\lambda_{\max}}[$ where $\lambda_{\max} \approx 6$. In this interval, the convergence rate of the HF modes remains close to one. Even the maximum of the decay factor of the LF part is large. In other

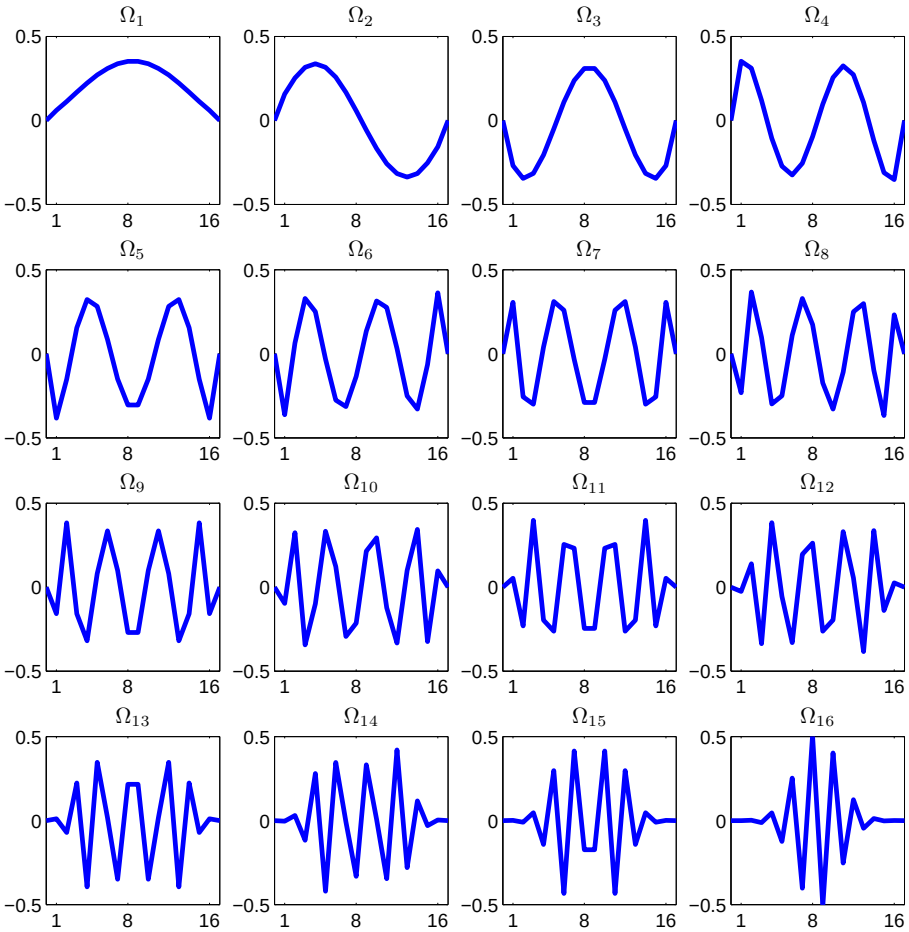

Figure 15: Bernstein — eigenvectors — $N = 16$

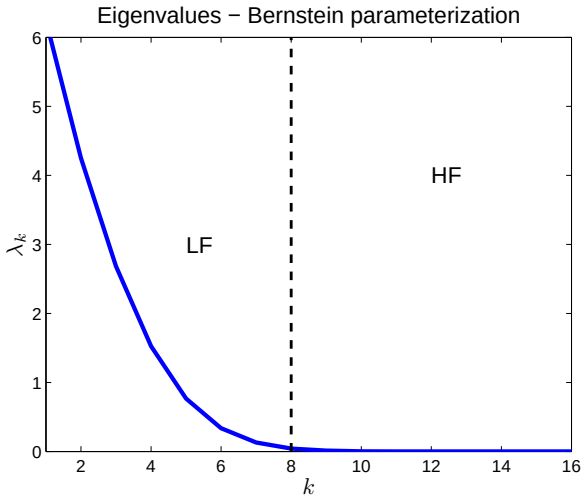

Figure 16: Bernstein — eigenvalues — $N = 16$

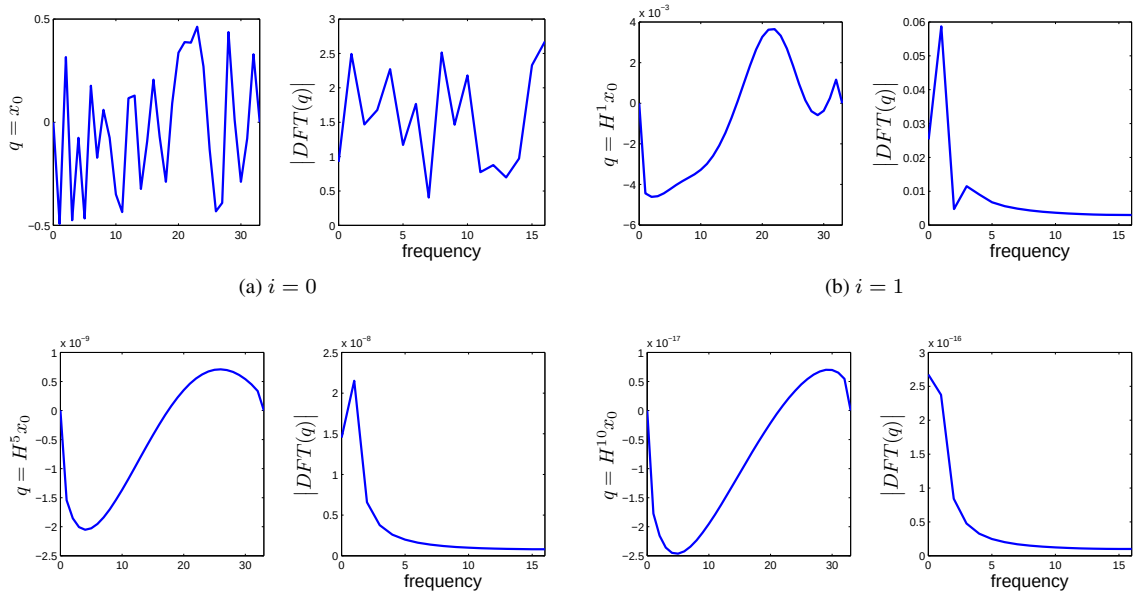

(a) $i = 0$ (b) $i = 1$

(c) $i = 5$ (d) $i = 10$

Figure 17: Krylov vectors $q^i = H^i x_0$ for the Bernstein parameterization — $N = 32$

words no solution operator can be efficient on the half of the space spanned by the LF modes. Consequently, the coarse parameterization space of an ideal two level algorithm must be redefined as a space of larger dimension than just the half of the fine space. For a multilevel algorithm, many intermediate levels should be considered.

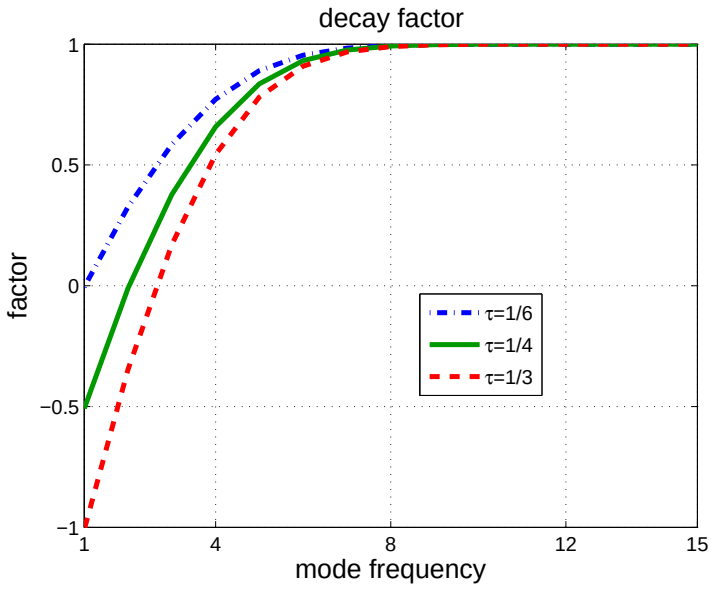

Figure 18: Decay function of a relaxed steepest descent method for the shape optimization problem in the Bernstein parameterization — $N = 15$.

5.2 B-splines parameterization

To our knowledge, we do not know any analytical form for the integral of two B-spline functions of degree d. However, since this product is a polynomial of degree $2d$, one can use an exact numerical quadrature using a $d + 1$ points Gaussian rule.

As for the Bézier parameterization, the constraints on the design vector are

$$x_0 = 0 \qquad \text{and} \qquad x_N = 0. \tag{67}$$

We assume that the problem has been scaled. The decay factors are computed after the numerical diagonalization of $D_H^{-1}H$ where D_H is the diagonal part of H, the projected Hessian. The Figures 19 and 20 depict the eigenvectors and the eigenvalues respectively. The results are close to the diagonalization obtained with the Bézier (Bernstein) parameterization.

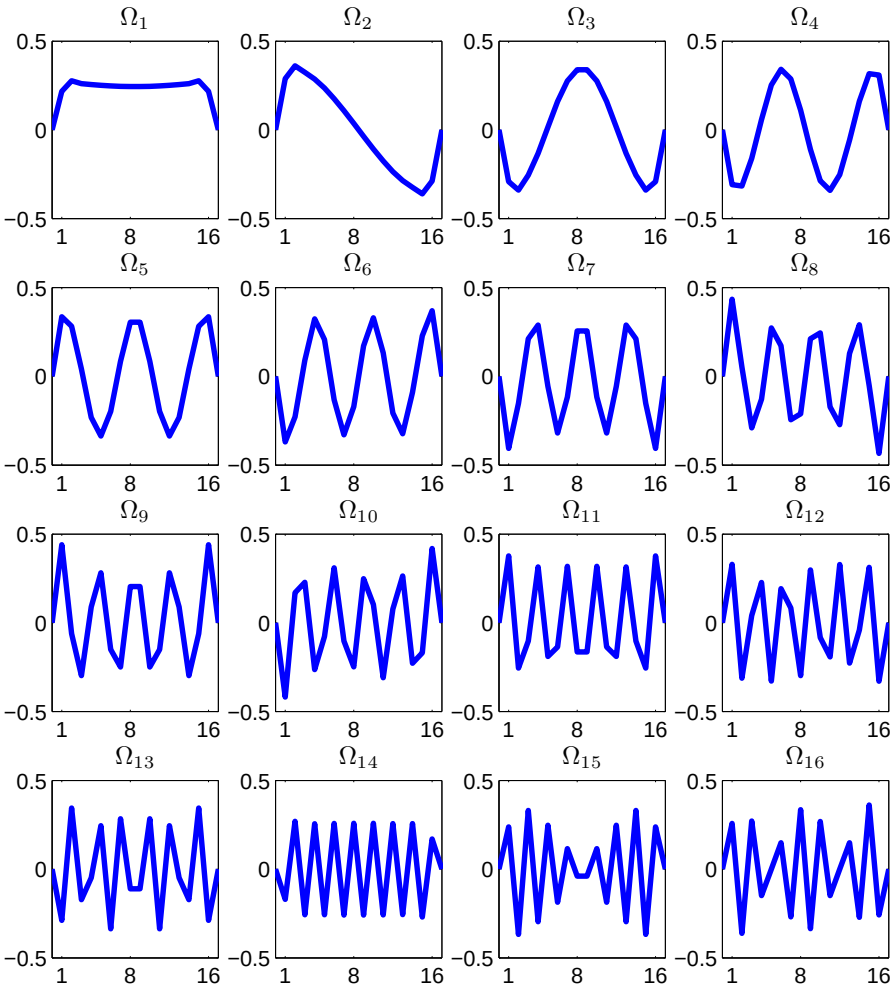

Figure 19: B-spline — eigenvectors — $N = 16$

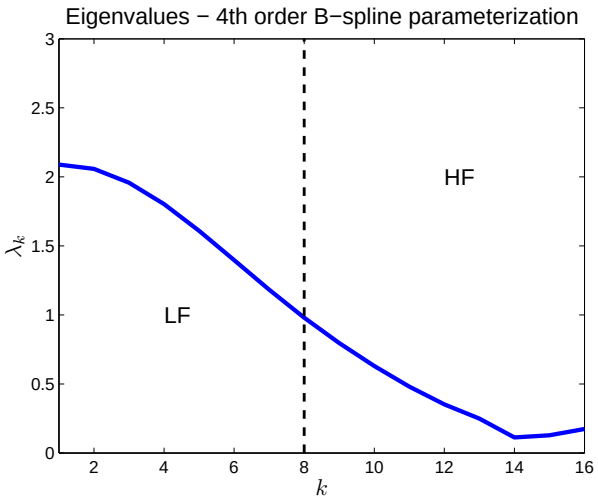

Figure 20: B-spline — eigenvalues — $N = 16$

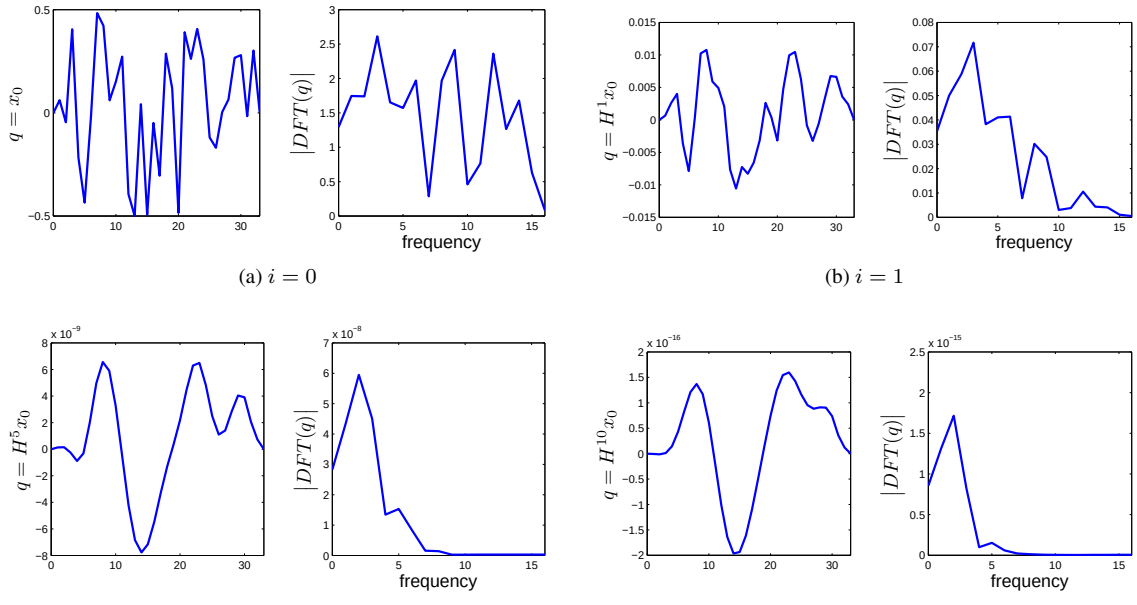

(a) $i = 0$ (b) $i = 1$

(c) $i = 5$ (d) $i = 10$

Figure 21: Krylov vectors with B-spline parameterization — $N = 32$

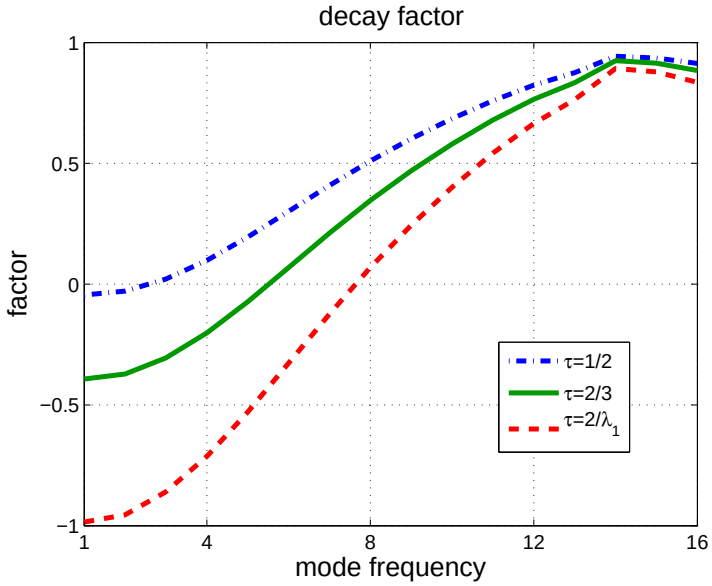

Figure 22: Decay factors of a relaxed steepest descent method for the shape optimization problem in the B-spline parameterization — $N = 16$.

5.3 Orthogonal polynomials

Let us recall a fundamental result related to the best approximation problem of a function $\bar{u} \in H_0$ in a subspace of polynomials of degree N on $[0\ 1]$, noted $\mathcal{P}^N$. First note that $\mathcal{P}^N$ is indeed a subspace of H_0 since $[0\ 1]$ is closed and bounded (compact, hence all continuous functions are L_2 integrable).

A basis of $\mathcal{P}^N$ that is orthogonal for the scalar product (1) is given by the Legendre polynomials noted P_k:

$$\int_{-1}^{1} P_k(t)P_j(t)dt = a_k\delta_{kj} \tag{68}$$

where δ_{kj} is the Kronecker symbol and $a_k = \frac{2}{2k+1}$.

The best approximation problem is trivial since the Hessian matrix H is diagonal with $h_{kk} = a_k$. The RHS coefficients $b_k = (\bar{u}, p_k)$ are the orthogonal projection of $\bar{u}$ on P_k and the inversion corresponds to the normalization by $a_k = \|P_k\|^2$ of every coefficients.

The spectrum and the conditioning of this system is obvious since it is diagonal. The eigenvectors (in terms of design parameters) are the canonical basis of $\mathbb{R}^{N+1}$ (Ω is the identity matrix), the eigenfunctions are the p_k functions, and the eigenvalues are the diagonal entries a_k. The condition number is given by $\kappa_2(H) = \frac{a_0}{a_n} = 2N + 1$.

Boundary conditions $u(0) = u(1) = 0$ read

$$\sum_{k=0}^{N} x_k = 0 \qquad \text{and} \qquad \sum_{k=0}^{N} (-1)^k x_k = 0. \tag{69}$$

5.4 Stiffness w.r.t. the space dimension

The inverse of the condition number can be seen as a distance to the closest non-invertible matrix [6]. In this sense, the greater the condition number, the more a matrix is numerically "hard" to invert, *i.e.* it is a stiff problem. In floating arithmetic, if this distance is of the order of the machine epsilon, it can be considered as a non-invertible matrix.

The Figure 23 depicts (a numerical estimation of the) condition numbers of Hessian matrices for several parameterizations (Bernstein, B-spline, Legendre, Tchebychev) w.r.t. the number of degrees of freedom.

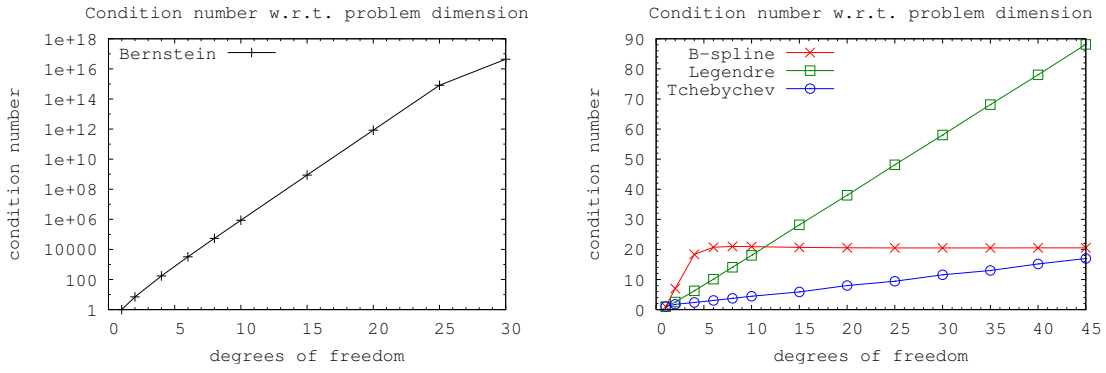

(a) Bernstein (logarithmic scale)

(b) Others (linear scale)

Figure 23: Comparison of the condition number of the Hessian matrix of the shape optimization problem for different parameterizations.

5.5 Numerical experiments

We aim at approaching the graph of the target function depicted in the Figure 24 with a Bézier curve of degree N. The target function is a sum of Gaussian functions (exponential). The target does not belong to any polynomial space. The accuracy of the optimal value J^* that can be achieved with our code is given by the shape obtained by orthogonal projection of the target function onto the space of polynomials of degree N (that is, in the Legendre basis). Thus, we can measure the convergences of the multilevel schemes in terms of the objective error $e \overset{\text{def.}}{=} J - J^*$.

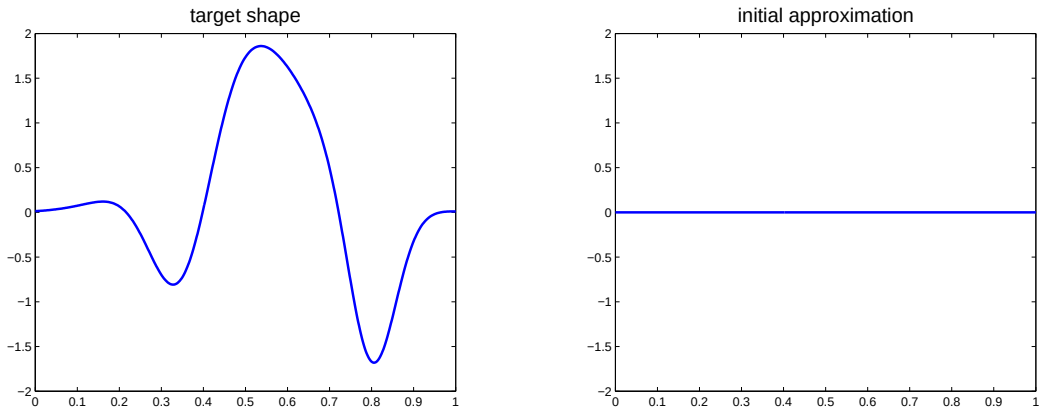

(a) target function

(b) initial function

Figure 24: Best approximation test-case description: the target function is a sum of Gaussian functions; the initial approximation is zero everywhere.

The fine parameterization is of degree $N = 24$. First we realize a numerical optimization with a classical method on the unique fine level. The results are illustrated in the Figure 25. This problem is effectively very stiff: the convergence is linear with a convergence rate close to 1.

The multilevel strategies are tested with two schemes: a *saw-tooth* cycle and a *V*-cycle. In addition, in the framework of an optimization problem, we will not consider that the problem has been scaled beforehand. A line search procedure is used at each descent iteration. The algorithm is stopped if it does not converge within 1000 functions evaluations.

The settings of the multilevel schemes are:

- parameterization degrees: $N = 3, 6, 9, 12, 15, 18, 21, 24$ (8 levels)
- pre-relaxation: $\nu_1 = 2$ iterations of Conjugate Gradient (Polak-Ribière, CG)
- post-relaxation: $\nu_2 = 2$ CG iterations (V-cycle only)

5.5.1 *Saw-tooth* cycle

The results are presented in the Figures 26, 27 and 28, resp. for the following transfers: a) classical, b) with spectrum permutation, c) algebraic. We observe that the classical strategy is useless: the error is of the same order as with the single level strategy and the convergence rate tends to 1. On the contrary, the other strategies are more efficient: the cost function at convergence is smaller with a convergence rate significantly smaller than 1 (≈ 0.70). The uniform error is 25 times smaller. The algebraic method ($J - J^* \approx 10^{-8}$) seems better than the spectrum permutation method ($J - J^* \approx 10^{-6}$). For the latter, the convergence rate tends to 0.9 for the last cycles. The concluding Figure 29 depicts the convergence of the objective function for all methods.

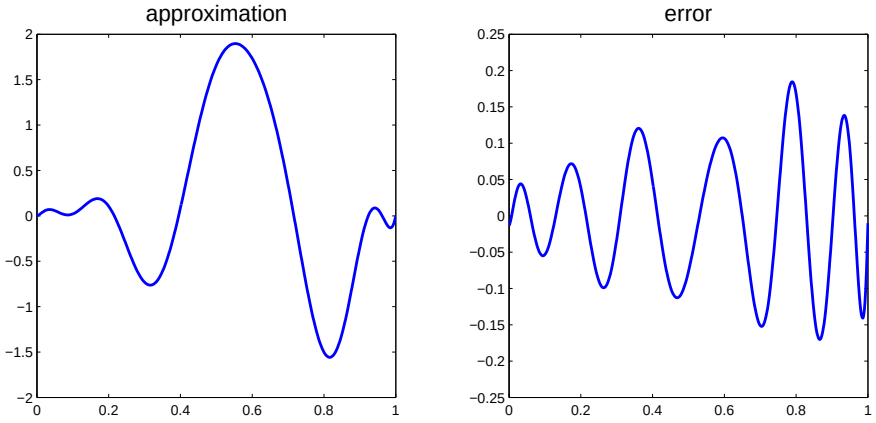

(a) approximation

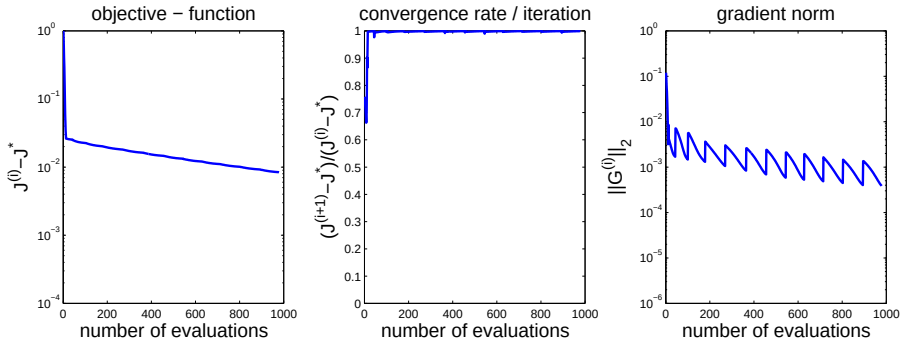

(b) convergence

Figure 25: CG (Polak-Ribière) method on the fine level.

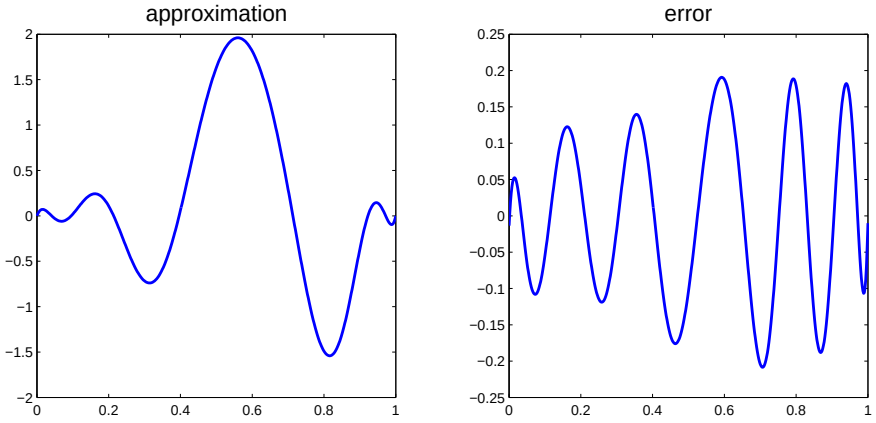

(a) approximation

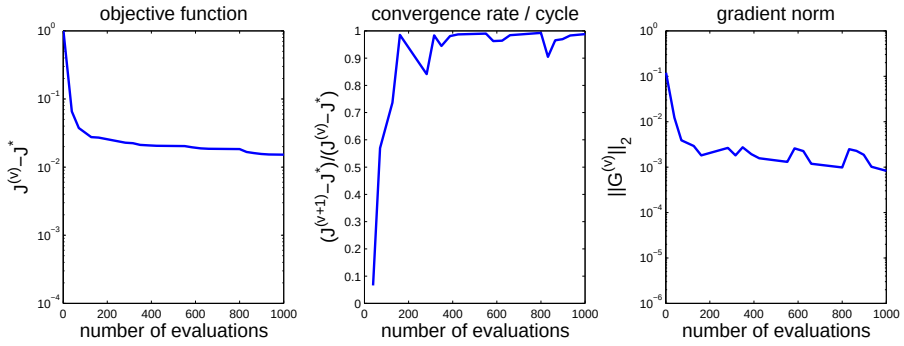

(b) convergence

Figure 26: classical transfer

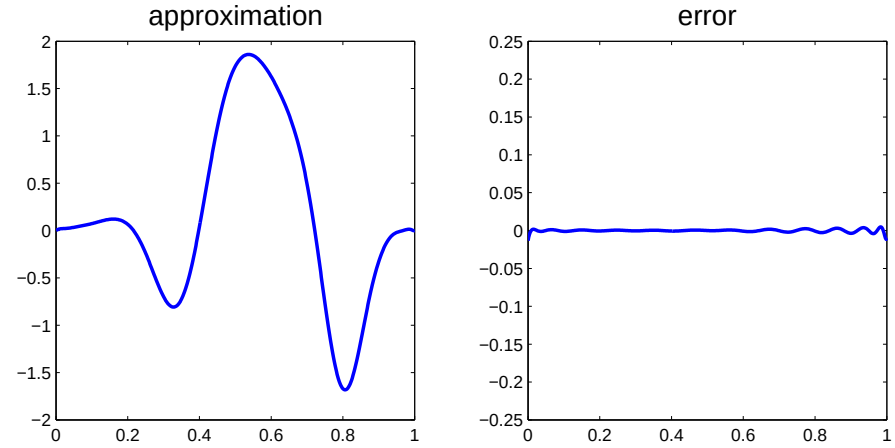

(a) approximation

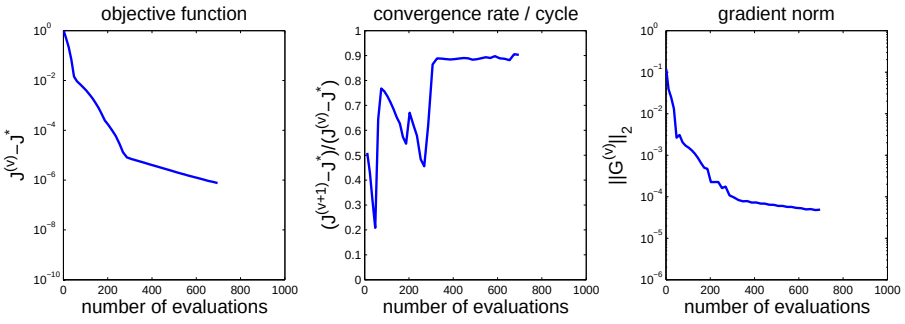

(b) convergence

Figure 27: spectrum permutation transfer

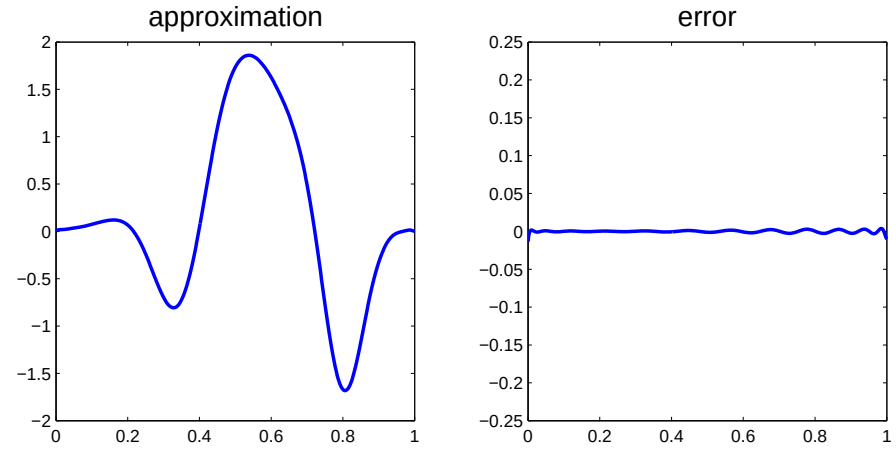

(a) approximation

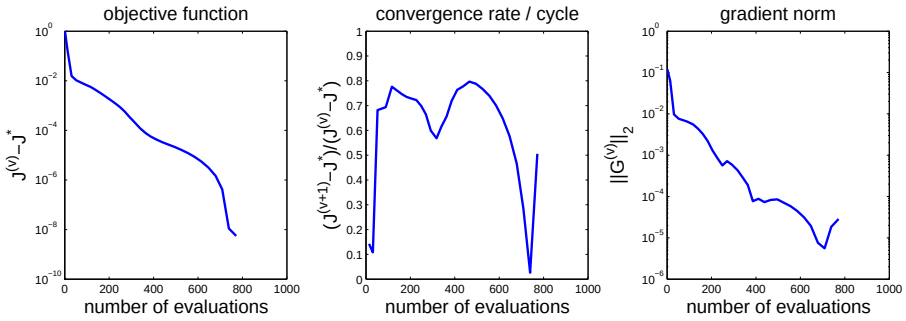

(b) convergence

Figure 28: algebraic transfer

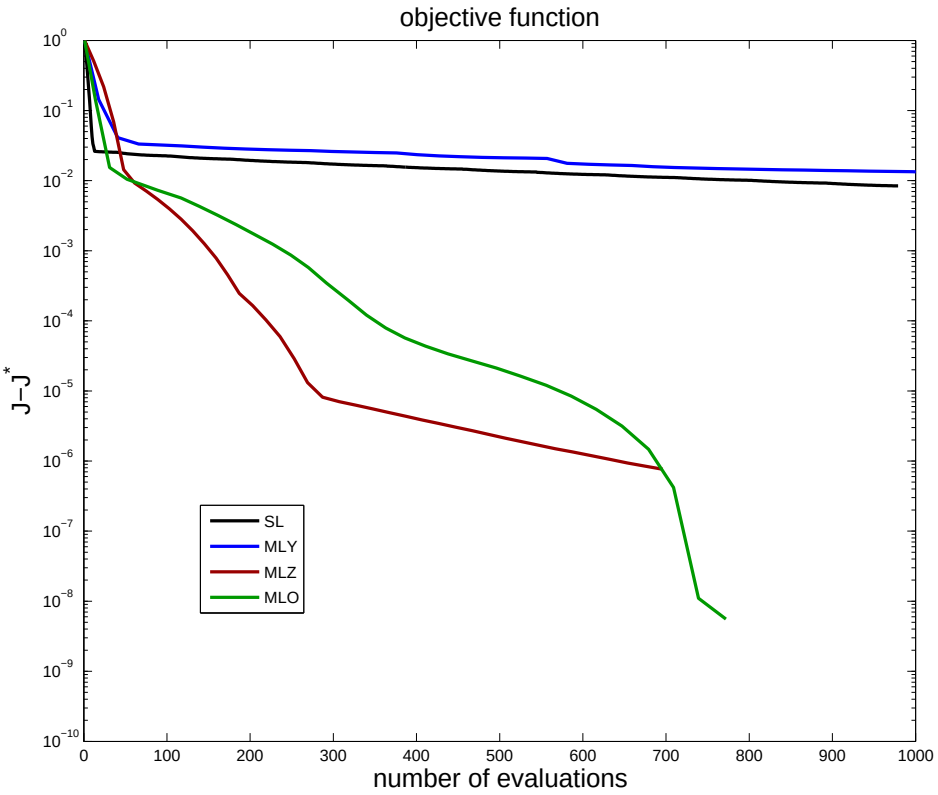

Figure 29: Convergence of the objective function for all multilevel strategies — saw-tooth cycle

5.5.2 Cycle en V

The results are presented in the Figures 30, 31 and 32, resp. for the transfers: a) classical, b) with spectrum permutation, c) algebraic. We observe the same results as for the saw-tooth scheme, as expected. The convergence of the objective function for all methods are depicted in the Figure 33.

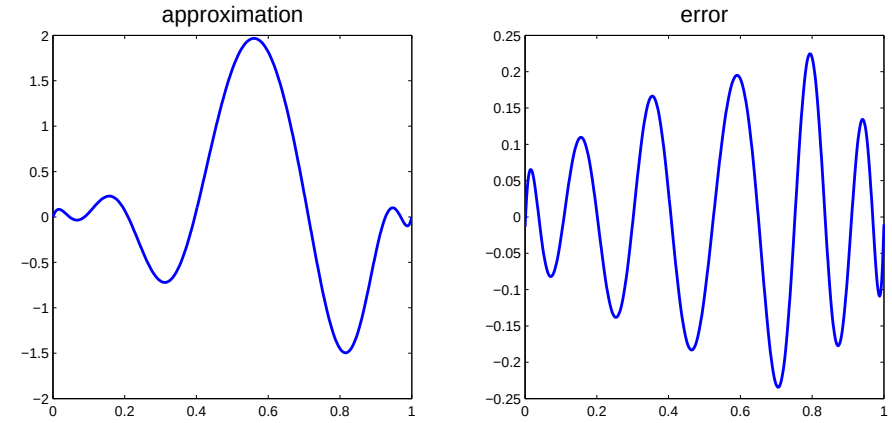

(a) approximation

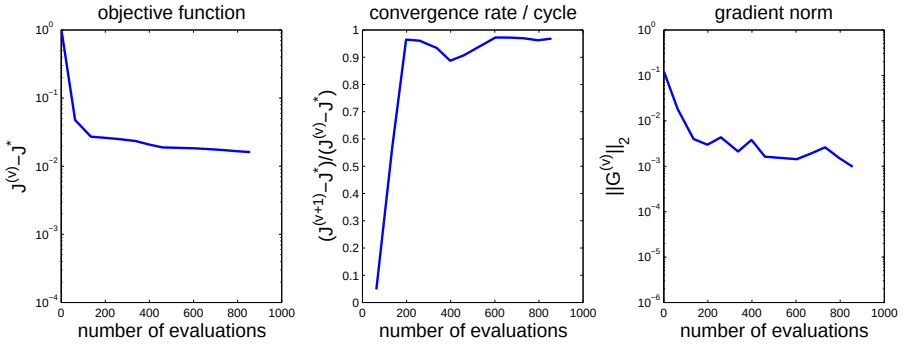

(b) convergence

Figure 30: classical transfer

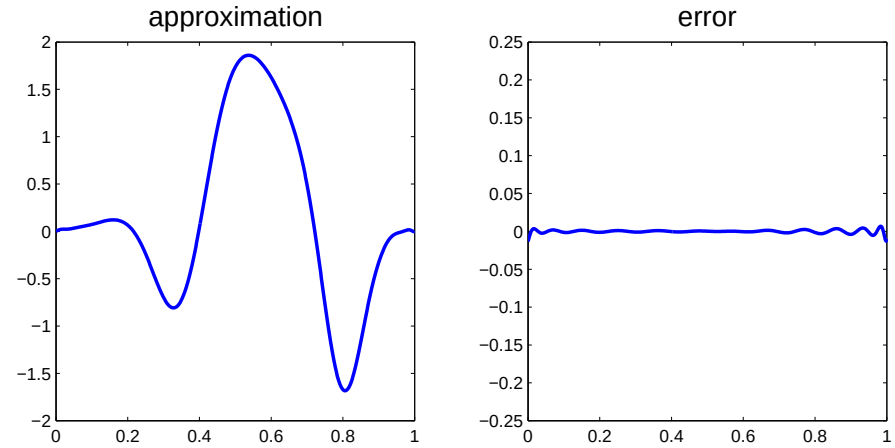

(a) approximation

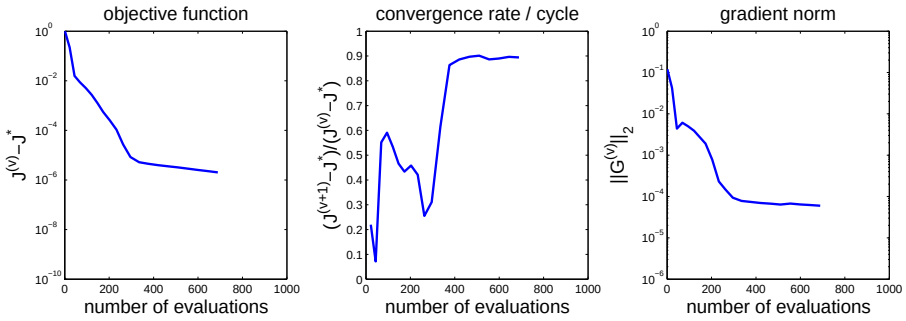

(b) convergence

Figure 31: spectrum permutation transfer

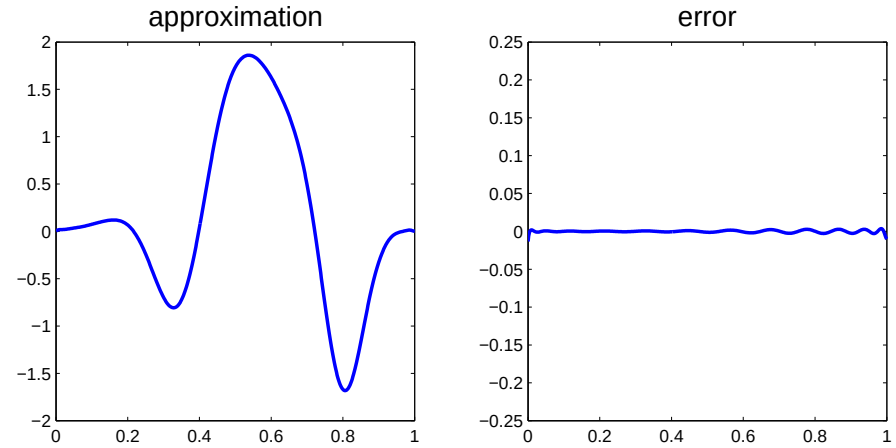

(a) approximation

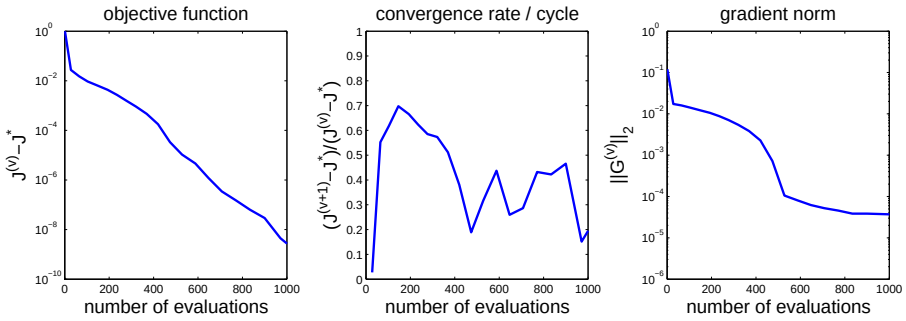

(b) convergence

Figure 32: algebraic transfer

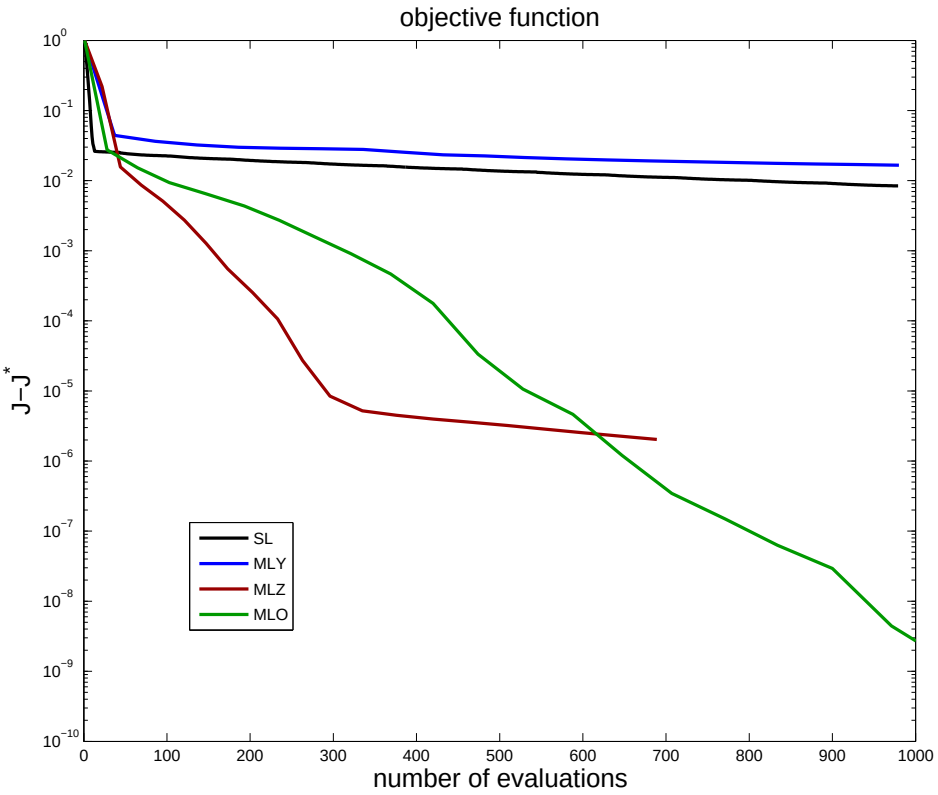

Figure 33: Convergence of the objective function for all multilevel strategies — V-Cycle

6 Conclusions and perspectives

The purpose of this paper was to show and illustrate how different can be stiff problems in the context of a PDE and in the context of a shape optimization problem. The behavior of the iterative methods for solving such problems are closely related to the nature of the linear operator: the Jacobian or the Hessian (depending on the context, PDE or optimization). In this article we have shown and illustrated these main differences; namely, they rely on their modal structure, closely related to the Fourier modes of discrete differential operators. As a consequence, these fundamental differences have a strong influence on the way the numerical treatment should be done, particularly regarding the preconditioning.

In the framework of PDE, multilevel preconditioning techniques are famous and very efficient, though sometimes hard to implement. For shape optimization problems, among them shape inverse problems, the multilevel preconditioning strategies are not always clearly established. This is partly due to additional difficulties that are intrinsic to optimization problems (for instance multimodality) but also to the shape representation (intrinsic geometry, mesh, parametric representation, etc.).

We have provided here an answer in the context of parametric shape inverse problems, taking into account the nature of the discrete integral operator. To make our analysis as close as possible to classical linear MG methods, we have used the same concepts (smoother, transfer operators, Coarse Grid Correction, etc.) and we have examined two-level ideal algorithms where the fine "grid" and the coarse "grid" are defined in a general abstract way, based on embedded parametric subspaces. Different kinds of transfer operators are proposed, extending the sense of a coarse grid. Using a steepest descent iteration (or equivalently a Jacobi iteration) as pre- and/or post-relaxation phase, a general form for the amplification matrix of the ideal cycle has been derived. In the particular case of piecewise linear functions, the amplification matrix of the ideal cycle is examined. Namely, the spectral radius is derived for each Coarse Grid Correction strategy. The following results are reported:

1. the classical CGC fails to improve the convergence rate: it remains mesh dependent and tends to the convergence rate of the unique relaxation phases; the "coarse grid" is composed of low frequency modes;

2. the alternative transfer operators (using spectrum permutation or eigenspace projection) provide a mesh independent convergence rate; the "coarse grid" is composed of high frequency modes.

To summarize, in order to provide a good preconditioner, possibly with multilevel techniques, one has to know the nature of the underlying operators. We could temper these results arguing that our specific problem is well-conditioned and that no preconditioning would be necessary. Indeed, though mesh dependent, the convergence rate is bounded above with the P1 parameterization whatever the mesh size (as theoretical argument we can advance that if for a PDE the Jacobian is the discrete form of a differential operator, which in the continuous formalism is not compact, on the contrary, the Hessian of the optimization problem is compact; so, apparently, we do not need any particular preconditioning). Nevertheless, this article rises the question of the parameterization with CAD techniques (such as Bézier representations of curves and surfaces). It appears that the parameterization deteriorates the conditioning. To complete this study we should analyse how the parameterization, which reduces considerably the number of design parameters, can be seen as a (bad) preconditioner itself. Furthermore, this properties are also important for other kind of preconditioner such as the BFGS method, which seems relevant in this case (there are few design parameters). Indeed a compact operator is easily approached by finite rank corrections and we could wonder how the parameterization can render this property difficult to achieve.

A Spectral radius of the ideal algorithms

A.1 Similarity transformations of the amplification matrix

A.1.1 Definition and properties

We recall the following similarity properties:

Definition 1. *Let A and B be two square matrices of same dimension. A and B are said to be similar if there exists an invertible matrix S such that $A = S^{-1}BS$. We note $A \sim B$.*

Theorem 2. *If $A \sim B$ then A and B have the same eigenvalues.*

Theorem 3. *Let A and B be two square matrices. Then $AB \sim BA$.*

A.1.2 Transformations

In section 4.2 we have derived the amplification matrix G of an ideal two-grid algorithm for both Poisson and shape optimization problem. G is of the form

$$G = G_\tau \left[I - P \left(RA_hP \right)^{-1} RA_h \right] G_\tau \tag{70}$$

where

$$\alpha R = P^T \tag{71}$$

for some positive α and

$$G_\tau = I - \frac{\tau}{\gamma} A_h. \tag{72}$$

Moreover we have the equalities $A_h = \beta_h A = \beta_h \Omega\Lambda\Omega$ and $A_{2h} = \beta_{2h} A' = \beta_{2h}\Omega'\Lambda'\Omega'$ with $\beta = \frac{\beta_h}{\beta_{2h}}$ independent of h.

Let us sketch similar transformations using the theorems of previous section.

$$\begin{aligned}
G &\sim \Omega G \Omega \\
&\quad \Omega G_\tau \Omega\Omega \left[I - P \left(RA_hP \right)^{-1} RA_h \right] \Omega\Omega G_\tau \Omega \\
&\quad (I - \frac{\tau}{\gamma}\Omega A\Omega) \left[I - \beta\Omega P (A')^{-1} R\Omega\Omega A\Omega \right] (I - \frac{\tau}{\gamma}\Omega A\Omega) \\
&\quad (I - \frac{\tau}{\gamma}\Lambda) \left[I - \alpha\beta\Omega R^T\Omega'\Lambda'^{-1}\Omega' R\Omega\Lambda \right] (I - \frac{\tau}{\gamma}\Lambda) \\
&\quad (I - \frac{\tau}{\gamma}\Lambda) \left[\Lambda^{-1} - \alpha\beta\Omega R^T\Omega'\Lambda'^{-1}\Omega' R\Omega \right] \Lambda (I - \frac{\tau}{\gamma}\Lambda) \\
&\sim \left[\Lambda^{-1} - \alpha\beta\Omega R^T\Omega'\Lambda'^{-1}\Omega' R\Omega \right] \Lambda (I - \frac{\tau}{\gamma}\Lambda)^2
\end{aligned}$$

Let D be the diagonal matrix such that $D_{kk} = d_k = \sqrt{\lambda_k}(1 - \frac{\tau}{\gamma}\lambda_k)$, *i.e.* $D = \Lambda^{\frac{1}{2}}(I - \frac{\tau}{\gamma}\Lambda) = (I - \frac{\tau}{\gamma}\Lambda)\Lambda^{\frac{1}{2}}$ and let $\sigma = \Omega' R \Omega$. We can write

$$G \sim \left[\Lambda^{-1} - \alpha\beta\sigma^T\Lambda'^{-1}\sigma \right] D^2 = \Sigma D^2$$

A.1.3 Structure of the Sigma matrix

Now we need evaluate Σ. We recall that we have two grids $\mathcal{T}_h$ and $\mathcal{T}_{2h}$ such that $h = \frac{1}{2^p} = \frac{1}{N+1}$ and $2h = \frac{1}{2^{p-1}} = \frac{1}{N'+1}$, *i.e.* $N = 2N' + 1$. Moreover we have the following property: let λ_k, $k = 1, \ldots, N$ be the eigenvalues on $\mathcal{T}_h$ and λ'_j, $j = 1, \ldots, N'$ be the eigenvalues on $\mathcal{T}_{2h}$. Then for all $j = 1, \ldots, N'$ we have $\lambda'_j = \lambda_{2j}$.

First we evaluate σ. Recall from (23) that $S_{ik} = \sqrt{\frac{2}{N+1}}\sin(ik\pi h) = \sqrt{2h}s_{ik}$.

$$\sigma = S'RS = 2\sqrt{2}hs'Rs \tag{73}$$

with $s'_{ik} = \sin(ik\pi 2h) = s_{2i,k} = s_{i,2k}$. Hence an element of $s'Rs$ reads

$$(s'Rs)_{jk} = \frac{1}{2\alpha}\sum_{i=1}^{N'} s_{2j,i}\left[s_{2i-1,k} + 2s_{2i,k} + s_{2i+1,k}\right] = \frac{1}{2\alpha}\tilde{\sigma}_{jk}. \tag{74}$$

Hence

$$\sigma = \frac{h\sqrt{2}}{\alpha}\tilde{\sigma}. \tag{75}$$

After trigonometric transformations (see [7] for instance) we find

$$\tilde{\sigma}_{jk} = \begin{cases} \frac{1}{h}\cos^2\left(\frac{\theta_k}{2}\right) & 1 \le j = k \le N' \\ -\frac{1}{h}\cos^2\left(\frac{\theta_k}{2}\right) & 1 \le j = N+1-k \le N' \\ 0 & \text{else} \end{cases} \tag{76}$$

Now that we have a simplified form for σ let us rewrite Σ

$$\Sigma = \Lambda^{-1} - \frac{\beta 2h^2}{\alpha}\tilde{\sigma}^T\Lambda'^{-1}\tilde{\sigma} = \frac{\beta 2h^2}{\alpha}C. \tag{77}$$

where

$$C_{jk} = \sum_{i=1}^{N'}\frac{\tilde{\sigma}_{i,j}\tilde{\sigma}_{i,k}}{\lambda_{2i}}, \qquad j,k = 1\dots N. \tag{78}$$

We consider the following different cases (see Figure 34):

(A) $j = k$

- **(A1)** $1 \le j = k \le N'$
- **(A2)** $N'+1 = j = k = N'+1$
- **(A3)** $N'+2 \le j = k \le N$

(B) $j = N+1-k$

(C) $j \ne k$ and $j \ne N+1-k$

According to (76) we deduce the following values for C_{jk}:

$$C_{jk} = \begin{cases} \dfrac{\cos^4\left(\frac{\theta_k}{2}\right)}{\lambda_{2k}h^2} & \textbf{A1} \\ 0 & \textbf{A2} \\ \dfrac{\cos^4\left(\frac{\theta_k}{2}\right)}{\lambda_{2(N+1-k)}h^2} & \textbf{A3} \\ -\dfrac{\cos^2\left(\frac{\theta_j}{2}\right)\cos^2\left(\frac{\theta_k}{2}\right)}{\lambda_{2j}h^2} & \textbf{B} \\ 0 & \textbf{C} \end{cases} \tag{79}$$

Finally, a general form for Σ is given:

$$\Sigma_{jk} = \begin{cases} \dfrac{1}{\lambda_k} - \dfrac{2\beta}{\alpha}\dfrac{\cos^4\left(\frac{\theta_k}{2}\right)}{\lambda_{2k}} & \textbf{A1} \\ \dfrac{1}{\lambda_k} & \textbf{A2} \\ \dfrac{1}{\lambda_k} - \dfrac{2\beta}{\alpha}\dfrac{\cos^4\left(\frac{\theta_k}{2}\right)}{\lambda_{2(N+1-k)}} & \textbf{A3} \\ \dfrac{2\beta}{\alpha}\dfrac{\cos^2\left(\frac{\theta_j}{2}\right)\cos^2\left(\frac{\theta_k}{2}\right)}{\lambda_{2j}} & \textbf{B} \\ 0 & \textbf{C} \end{cases} \tag{80}$$

It appears that Σ has non-zero values on the diagonal and the perdiagonal only.

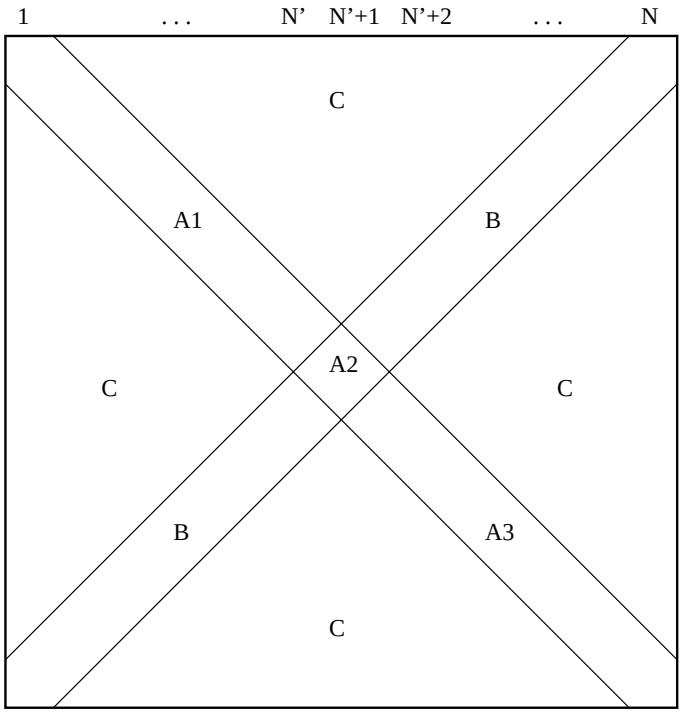

Figure 34: Structure of Σ

A.1.4 Application to the model problems

Poisson equation

- $\alpha = 2$
- $\beta = 4$
- $\lambda_k = 2 - 2\cos(\theta_k) = 4\sin^2(\frac{\theta_k}{2})$

A1: $1 \leq k \leq N'$

$$\begin{aligned}
\Sigma_{kk} &= \frac{1}{4\sin^2(\frac{\theta_k}{2})} - 4\frac{\cos^4(\frac{\theta_k}{2})}{4\sin^2(\theta_k)} \\
&= \frac{1}{4\sin^2(\frac{\theta_k}{2})} - \frac{\cos^4(\frac{\theta_k}{2})}{4\sin^2(\frac{\theta_k}{2})\cos^2(\frac{\theta_k}{2})} \\
&= \frac{1}{4}\frac{\cos^2(\frac{\theta_k}{2})(1-\cos^2(\frac{\theta_k}{2}))}{\sin^2(\frac{\theta_k}{2})\cos^2(\frac{\theta_k}{2})} \\
&= \frac{1}{4}
\end{aligned}$$

A2: $k = N' + 1 = \frac{1}{2h}$

$$\begin{aligned}
\Sigma_{kk} &= \frac{1}{4\sin^2(\frac{\theta_k}{2})} \\
&= \frac{1}{4\sin^2(\frac{\pi}{4})} \\
&= \frac{1}{2}
\end{aligned}$$

A3: $N' + 2 \leq k \leq N$

$$\begin{aligned}
\Sigma_{kk} &= \frac{1}{4\sin^2(\frac{\theta_k}{2})} - 4\frac{\cos^4(\frac{\theta_k}{2})}{4\sin^2((N+1-k)\pi h)} \\
&= \frac{1}{4\sin^2(\frac{\theta_k}{2})} - 4\frac{\cos^4(\frac{\theta_k}{2})}{4\sin^2(\theta_k)} \\
&= \frac{1}{4}
\end{aligned}$$

B: $1 \leq j = N + 1 - k = \frac{1}{h} - k \leq N'$

$$\begin{aligned}
\Sigma_{jk} &= 4\frac{\cos^2\left(\frac{\theta_j}{2}\right)\cos^2\left(\frac{\theta_k}{2}\right)}{4\sin^2(\theta_j)} \\
&= \frac{\cos^2\left(\frac{\theta_j}{2}\right)\cos^2\left(\frac{\theta_k}{2}\right)}{4\sin^2(\frac{\theta_j}{2})\cos^2(\frac{\theta_j}{2})} \\
&= \frac{1}{4}\frac{\cos^2\left(\frac{\theta_k}{2}\right)}{\sin^2(\frac{\pi}{2} - \frac{\theta_k}{2})} \\
&= \frac{1}{4}
\end{aligned}$$

$$\Sigma_{kj} = \Sigma_{jk}$$

Shape optimization

- $\alpha = 1$
- $\beta = \frac{1}{2}$

- $\lambda_k = 4 + 2\cos(\theta_k)$

A1: $1 \leq k \leq N'$

$$\Sigma_{kk} = \frac{1}{\lambda_k} - \frac{\cos^4(\frac{\theta_k}{2})}{\lambda_{2k}}$$

A2: $k = N' + 1 = \frac{1}{2h}$

$$\begin{aligned}\Sigma_{kk} &= \frac{1}{4 + 2\cos(\theta_k)} \\ &= \frac{1}{4 + 2\cos(\frac{\pi}{2})} \\ &= \frac{1}{4}\end{aligned}$$

A3: $N' + 2 \leq k \leq N$

$$\begin{aligned}\Sigma_{kk} &= \frac{1}{\lambda_k} - \frac{\cos^4(\frac{\theta_k}{2})}{4 + 2\cos(2(N+1-k)\pi h)} \\ &= \frac{1}{\lambda_k} - \frac{\cos^4(\frac{\theta_k}{2})}{\lambda_{2k}}\end{aligned}$$

B: $1 \leq k = N + 1 - j \leq N'$

$$\Sigma_{jk} = \frac{\sin^2\left(\frac{\theta_k}{2}\right)\cos^2\left(\frac{\theta_k}{2}\right)}{\lambda_{2k}}$$

$$\Sigma_{kj} = \Sigma_{jk}$$

A.2 Spectral radius of the Poisson problem with classical transfer

Recall that $A_h = \frac{1}{h^2}A = \frac{1}{h^2}\Omega\Pi\Omega$ and $A_{2h} = \frac{1}{4h^2}A' = \frac{1}{4h^2}\Omega'\Pi'\Omega'$. Let R be the mean operator $R = \frac{1}{2}P^T$ such that $RA_hP = A_{2h}$. According to the Appendix A.1 we have the following similarity property

$$G \sim \left[\Pi^{-1} - 8\sigma^T{\Pi'}^{-1}\sigma\right] D^2 = \Sigma D^2$$

with $D = \Pi^{\frac{1}{2}}(I - \frac{\tau}{2}\Pi)$, $\sigma = \Omega' R \Omega$, and

$$\Sigma = \begin{pmatrix} \frac{1}{4} & & & & & & & & \frac{1}{4} \\ & \frac{1}{4} & & & & & & \frac{1}{4} & \\ & & \ddots & & & & \iddots & & \\ & & & \frac{1}{4} & & \frac{1}{4} & & & \\ & & & & \frac{1}{2} & & & & \\ & & & \frac{1}{4} & & \frac{1}{4} & & & \\ & & \iddots & & & & \ddots & & \\ & \frac{1}{4} & & & & & & \frac{1}{4} & \\ \frac{1}{4} & & & & & & & & \frac{1}{4} \end{pmatrix}. \tag{81}$$

Therefore G is similar to

$$\Sigma D^2 = \frac{1}{4}\begin{pmatrix} d_1^2 & & & & & & & & d_N^2 \\ & d_2^2 & & & & & & d_{N-1}^2 & \\ & & \ddots & & & & \iddots & & \\ & & & d_{N'} & & d_{N'+2}^2 & & & \\ & & & & 2d_{N'+1}^2 & & & & \\ & & & d_{N'}^2 & & d_{N'+2}^2 & & & \\ & & \iddots & & & & \ddots & & \\ & d_2^2 & & & & & & d_{N-1}^2 & \\ d_1^2 & & & & & & & & d_N^2 \end{pmatrix}. \tag{82}$$

We now need to provide the eigenpairs $(\mathbf{w}_k, \alpha_k)$ of ΣD^2. Let $\mathbf{e}_k$ be the canonical vectors, $\mathbf{e}_{jk} = \delta_{jk}$. Three cases are distinguished:

i) First let $k \leq N'$ and $\mathbf{w}_k = \mathbf{e}_k + \mathbf{e}_{N+1-k}$. It is easy to check that $\mathbf{w}_k$ is an eigenvector with eigenvalue $\alpha_k = \frac{1}{4}(d_k^2 + d_{N+1-k}^2)$.

ii) Then it is clear that the vector $\mathbf{w}_{N'+1} = \mathbf{e}_{N'+1}$ is an eigenvector associated to the eigenvalue $\alpha_{N'+1} = \frac{1}{2}d_{N'+1}^2$.

iii) Finally let $k \geq N' + 2$ and $\mathbf{w}_k = d_{N+1-k}^2\mathbf{e}_k - d_k^2\mathbf{e}_{N+1-k}$. It is easy to check that all $\mathbf{w}_k$ are non-zero vectors that belong to the null space of ΣD^2. Hence they are k eigenvectors associated to the eigenvalue $\alpha_k = 0$.

Since all the N vectors $\mathbf{w}_k$ defined above are linearly independent, we deduce that all eigenpairs have been found. Therefore the spectral radius of the MG cycle reads

$$\begin{aligned} \rho(\Sigma D^2) &= \max_{k=1..N} |\alpha_k| \\ &= \tfrac{1}{4} \max_{k=1..N'+1} d_k^2 + d_{N+1-k}^2 \end{aligned}$$

Let $\tau = \frac{2}{3}$ to define the optimal solution operator on the HF subspace (optimal smoother, see section 3.4). Since

$$\begin{aligned} d_k^2 &= \mu_k \left(1 - \tfrac{\tau}{2}\mu_k\right)^2 \\ &= 2\left(1 - \cos\theta_k\right)\left(1 - \tfrac{2}{3}(1 - \cos\theta_k)\right)^2 \\ &= \tfrac{2}{9}\left(1 - \cos\theta_k\right)\left(1 + 2\cos\theta_k\right)^2 \end{aligned}$$

then

$$\begin{aligned} \tfrac{9}{2}\left(d_k^2 + d_{N+1-k}^2\right) &= \left(1 - \cos\theta_k\right)\left(1 + 2\cos\theta_k\right)^2 + \left(1 + \cos\theta_k\right)\left(1 - 2\cos\theta_k\right)^2 \\ &= \left(1 + 2\cos\theta_k\right)^2 + \left(1 - 2\cos\theta_k\right)^2 \\ &\quad + \cos\theta_k\left(\left(1 + 2\cos\theta_k\right)^2 - \left(1 - 2\cos\theta_k\right)^2\right) \\ &= 2\left(1 + 4\cos^2\theta_k\right) - 8\cos^2\theta_k \\ &= 2 \end{aligned}$$

Hence

$$\rho(\Sigma D^2) = \frac{1}{4}\frac{4}{9} = \frac{1}{9}. \tag{83}$$

The spectral radius of one ideal cycle is independent from the mesh size (and smaller than 1). Hence this method has a fast convergence whatever the mesh size.

A.3 Spectral radius of the shape optimization problem with classical transfer

Recall that $H_h = \frac{h}{6}B = \frac{h}{6}\Omega\Lambda\Omega$ and $H_{2h} = \frac{2h}{6}B' = \frac{2h}{6}\Omega'\Lambda'\Omega'$. To coincide with the notations of the previous analysis we will write the transfer in terms of the restriction operator. According to the section A.1 we have the similarity property

$$G \sim \left[\Lambda^{-1} - \frac{1}{2}\sigma^T {\Lambda'}^{-1}\sigma\right] D^2 = \Sigma D^2$$

with $D = \Lambda^{\frac{1}{2}}(I - \frac{\tau}{4}\Lambda)$, $\sigma = \Omega' R \Omega$, and

$$\Sigma_{jk} = \begin{cases} \dfrac{1}{\lambda_k} - \dfrac{\cos^4\left(\frac{\theta_k}{2}\right)}{\lambda_{2k}} & j = k \neq N'+1 \\ \dfrac{1}{4} & j = k = N'+1 \\ \dfrac{\cos^2\left(\frac{\theta_k}{2}\right)\sin^2\left(\frac{\theta_k}{2}\right)}{\lambda_{2k}} & j + k = N+1 \\ 0 & \text{else} \end{cases} . \tag{84}$$

Σ, and consequently ΣD^2, have the structure depicted in the Figure 34. Let $\tau = \frac{4}{5}$ for a sake of consistency with the section 3. The values of the diagonal matrix D^2 are

$$\begin{aligned} d_k^2 &= \lambda_k\left(1 - \tfrac{\tau}{4}\lambda_k\right)^2 \\ &= \lambda_k\left(1 - \tfrac{1}{5}\left(4 + 2\cos\theta_k\right)\right)^2 \\ &= \tfrac{1}{25}\lambda_k\left(1 - 2\cos\theta_k\right)^2 . \end{aligned}$$

Thus the non-zero entries of ΣD^2 read

i) $j = k \neq N'+1$

$$\begin{aligned} (\Sigma D^2)_{kk} &= \frac{1}{25}\left(\frac{1}{\lambda_k} - \frac{\cos^4\left(\frac{\theta_k}{2}\right)}{\lambda_{2k}}\right)\lambda_k\left(1 - 2\cos\theta_k\right)^2 \\ &= \frac{1}{25}\frac{\lambda_{2k} - \lambda_k\cos^4\left(\frac{\theta_k}{2}\right)}{\lambda_{2k}}\left(1 - 2\cos\theta_k\right)^2 \end{aligned}$$

ii) $j = k = N'+1$

$$\begin{aligned} (\Sigma D^2)_{N'+1,N'+1} &= \frac{1}{25}\frac{1}{4}\lambda_{N'+1}\left(1 - 2\cos\tfrac{\pi}{2}\right)^2 \\ &= \frac{1}{25}\frac{1}{4}4 \\ &= \frac{1}{25} \end{aligned}$$

iii) $j + k = N+1$

$$(\Sigma D^2)_{jk} = \frac{1}{25}\frac{\cos^2\left(\frac{\theta_k}{2}\right)\sin^2\left(\frac{\theta_k}{2}\right)}{\lambda_{2k}}\lambda_k\left(1 - 2\cos\theta_k\right)^2$$

Let us derive the eigenpairs of ΣD^2. One eigenpair is obvious: for $k = N'+1$, it is easy to check that $\mathbf{w}_k = \mathbf{e}_k$ is an eigenvector associated to the eigenvalue $\alpha_k = \frac{1}{25}$. The expression of the other $N - 1 = 2N'$ eigenvectors of ΣD^2 is not as straightforward as for the Poisson equation. To derive them we adopt the following strategy: first we make an ansatz for the eigenvectors $\mathbf{w}_k$ and deduce linear systems

to be solved; then these systems are solved using the symbolic calculations software Maple©; finally the linear independence of the solutions is verified.

For all $k \leq N'$ assume that $\mathbf{w}_k$ has the structure $\mathbf{w}_k = x_k \mathbf{e}_k + x_{N+1-k}\mathbf{e}_{N+1-k}$:

$$\mathbf{w}_k = \begin{pmatrix} & \\ x_k & \\ & \\ & \\ x_{N+1-k} & \\ & \end{pmatrix}.$$

We can assume w.l.o.g. that $x_{N+1-k} = 1$ since all eigenvectors are defined up to a multiplicative constant (equivalently we can assume that the eigenvectors are normalized, $x_k^2 + x_{N+1-k}^2 = 1$, and choose $x_k \geq 0$). For each $\mathbf{w}_k$ the following linear system has to be solved:

$$(\Sigma D^2)\mathbf{w}_k = \alpha_k \mathbf{w}_k. \tag{85}$$

Injecting the ansatz in (85) gives the system

$$\left\{ \begin{array}{lcll} x_k(\Sigma D^2)_{k,k} & + & (\Sigma D^2)_{k,N+1-k} & = \alpha_k x_k \\ x_k(\Sigma D^2)_{N+1-k,k} & + & (\Sigma D^2)_{N+1-k,N+1-k} & = \alpha_k \end{array} \right.$$

whose unknowns are x_k and α_k. We have thus defined N' linear systems for $k = 1, \ldots, N'$. Each system can be written as a 2nd order equation in x_k and a linear equation in α_k. It follows that there are 2 pairs of solutions for each system, if they exist: the remaining $2N'$ eigenpairs.

According to Maple we obtain the following result:

i) The N' linearly independent vectors

$$\begin{array}{rcl} \mathbf{w}_k & = & \cos^2\left(\frac{\theta_k}{2}\right)\left(1 - 8\cos^2\left(\frac{\theta_k}{2}\right) + 16\cos^4\left(\frac{\theta_k}{2}\right)\right)\mathbf{e}_k \\ & & -\sin^2\left(\frac{\theta_k}{2}\right)\left(1 - 8\sin^2\left(\frac{\theta_k}{2}\right) + 16\sin^4\left(\frac{\theta_k}{2}\right)\right)\mathbf{e}_{N+1-k} \end{array}$$

belong to the null space. They are eigenvectors with eigenvalue $\alpha_k = 0$.

ii) The N' linearly independent vectors

$$\begin{array}{rcl} \mathbf{w}_{N'+1+k} & = & \sin^2\left(\frac{\theta_k}{2}\right)\left(1 + 2\sin^2\left(\frac{\theta_k}{2}\right)\right)\mathbf{e}_k \\ & & +\cos^2\left(\frac{\theta_k}{2}\right)\left(1 + 2\cos^2\left(\frac{\theta_k}{2}\right)\right)\mathbf{e}_{N+1-k} \end{array}$$

are eigenvectors associated to the eigenvalues

$$\alpha_{N'+1+k} = \frac{1}{25}\frac{27 - 144\cos^2\left(\frac{\theta_k}{2}\right) + 304\cos^4\left(\frac{\theta_k}{2}\right) - 320\cos^6\left(\frac{\theta_k}{2}\right) + 160\cos^8\left(\frac{\theta_k}{2}\right)}{3 - 8\cos^2\left(\frac{\theta_k}{2}\right) + 8\cos^4\left(\frac{\theta_k}{2}\right)}.$$

The spectral radius of this ideal cycle read

$$\begin{array}{rcl} \rho(\Sigma D^2) & = & \max\limits_{k=1..N} |\alpha_k| \\ & = & \max\limits_{k=N'+1..N} |\alpha_k| \end{array}$$

One can show that $\alpha_k > \frac{1}{25}$ for $k = 1 \ldots N'$ and that α is a monotonous decreasing function of $\theta \in]0\ \frac{\pi}{2}[$. Hence the max is attained for $\theta = \theta_1$, *i.e.* $\rho(\Sigma D^2) = \alpha_{N'+2}$ which is mesh dependent. When the mesh size tends to 0 ($h \to 0$) we have $\alpha_{N'+2} \to \frac{9}{25} = (\frac{3}{5})^2$. This is exactly the behavior of 2 Jacobi iterations (see 3.4). This means that the coarse subproblem is useless.

A.4 Spectral radius of the shape optimization problem with alternative transfer

Let us consider P1 parameterizations for all levels and $E^N_{N'} = P$. We conduct a spectral analysis of the amplification matrix (50) with $Q = \Omega\mathbb{P}\Omega^T P$ in order to compute its spectral radius. The calculations follow this outline:

a) The expression of the coarse problem $H' = Q^T H_h Q$ is simplified.

b) A simple form for $I - QH'^{-1}Q^T H_h$ is deduced and similar transformations are applied to G; it follows that G is similar to some matrix ΣD^2 where D is diagonal.

c) The entries of Σ are computed and exhibit a structure depicted in the Figure 34.

d) An ansatz for the eigenvectors of ΣD^2 is proposed and the resulting linear systems are solved with the help of Maple. We deduce a closed form for the eigenvalues and consequently the spectral radius.

Recall that $H_h = \beta_h B = \beta_h \Omega\Lambda\Omega^T$ and $G_\tau = I - \frac{\tau}{4}B$.

a The matrix of the coarse problem reads

$$\begin{aligned} Q^T H_h Q &= \beta_h P^T \Omega\mathbb{P}\Omega^T \Omega\Lambda\Omega^T \Omega\mathbb{P}\Omega^T P \\ &= \beta_h P^T \Omega\mathbb{P}\Lambda\mathbb{P}\Omega^T P \\ &= \beta_h P^T C P \end{aligned}$$

where we have noted $C = \Omega\mathbb{P}\Lambda\mathbb{P}\Omega^T$. The product $\Omega\mathbb{P}$ permutes the columns and the product $\mathbb{P}\Omega$ permutes the lines. Recall (section 2.3) that the eigenvectors S_k have the following symmetry: if k is odd, then S_k is even w.r.t. middle value and conversely if k is even, then S_k is odd w.r.t. middle value. Formally this reads

$$S_{(N+1-j)k} = \begin{cases} S_{jk} & k \text{ odd} \\ -S_{jk} & k \text{ even} \end{cases}$$

Thus we have

$$\Omega\mathbb{P} = \begin{pmatrix} S_N & \cdots & S_1 \end{pmatrix} \qquad \mathbb{P}\Omega = \begin{pmatrix} S_1 & -S_2 & S_3 & \cdots & -S_{N-1} & S_N \end{pmatrix}.$$

Moreover we have $(\mathbb{P}\Omega)^T = \Omega\mathbb{P}$, hence

$$C = \Omega\mathbb{P}\Lambda\mathbb{P}\Omega^T = \begin{pmatrix} S_1^T \\ -S_2^T \\ \vdots \\ -S_{N-1}^T \\ S_N^T \end{pmatrix} \begin{pmatrix} \lambda_1 & & \\ & \ddots & \\ & & \lambda_N \end{pmatrix} \begin{pmatrix} S_1 & -S_2 & \cdots & -S_{N-1} & S_N \end{pmatrix}.$$

$$\begin{aligned} C_{jk} &= \sum_{i=1}^{N} \lambda_i \, (-1)^{j+k} \, s_{ij} s_{ik} \\ &= 2h \, (-1)^{j+k} \sum_{i=1}^{N} (4 + 2\cos\theta_i) \sin(i\theta_j) \sin(i\theta_k) \end{aligned}$$

The orthogonality of the eigenvectors yields

$$\begin{aligned} \sum_{i=1}^{N} 4 \sin(i\theta_j) \sin(i\theta_k) &= \frac{4}{2h}\delta_{jk} \\ \sum_{i=1}^{N} 2\cos(\theta_i) \sin(i\theta_j) \sin(i\theta_k) &= \frac{1}{2h}(\delta_{j,k-1} + \delta_{j,k+1}) \end{aligned}$$

Hence

$$C = \begin{pmatrix} 4 & -1 & & & \\ -1 & 4 & -1 & & \\ & & \ddots & & \\ & & -1 & 4 & -1 \\ & & & -1 & 4 \end{pmatrix}.$$

Finally, straightforward multiplications with the linear interpolation operator gives

$$Q^T H_h Q = \beta_h P^T C P = 4\beta_h I \tag{86}$$

b According to (86) we have

$$\begin{aligned} I - Q(Q^T H_h Q)^{-1} Q^T H_h &= I - \frac{1}{4\beta_h} Q Q^T \beta_h \Omega\Lambda\Omega \\ &= I - \frac{1}{4}\Omega\mathbb{P}\Omega P P^T \Omega\mathbb{P}\Lambda\Omega \end{aligned}$$

Let us apply similar transformations on G using the property that Ω is symmetrical and orthogonal:

$$\begin{aligned} G &= G_\tau \left[I - Q \left(Q^T H_h Q\right)^{-1} Q^T H_h \right] G_\tau \\ &= G_\tau \Omega\Omega \left[I - \frac{1}{4}\Omega\mathbb{P}\Omega P P^T \Omega\mathbb{P}\Lambda\Omega \right] \Omega\Omega G_\tau \\ &= G_\tau \Omega \left[I - \frac{1}{4}\mathbb{P}\Omega P P^T \Omega\mathbb{P}\Lambda \right] \Lambda^{-1}\Lambda\Omega G_\tau \\ &\sim \Omega G_\tau \Omega \left[\Lambda^{-1} - \frac{1}{4}\mathbb{P}\Omega P P^T \Omega\mathbb{P} \right] \Lambda\Omega G_\tau \Omega \\ &\sim \left[\Lambda^{-1} - \frac{1}{4}\mathbb{P}\Omega P P^T \Omega\mathbb{P} \right] \Lambda(I - \frac{\tau}{4}\Lambda)^2 = \Sigma D^2 \end{aligned}$$

where we have noted

$$\begin{aligned} \Sigma &= \left[\Lambda^{-1} - \tfrac{1}{4}\mathbb{P}\Omega P P^T \Omega\mathbb{P}\right] \\ D^2 &= \Lambda(I - \tfrac{\tau}{4}\Lambda)^2 \end{aligned} \tag{87}$$

Moreover, since $\mathbb{P}$ is orthogonal we have $G \sim (\mathbb{P}\Sigma\mathbb{P})(\mathbb{P}D^2\mathbb{P})$ and

$$\begin{aligned} \mathbb{P}\Sigma\mathbb{P} &= \left[\mathbb{P}\Lambda^{-1}\mathbb{P} - \tfrac{1}{4}\Omega P P^T \Omega\right] \\ \mathbb{P}D^2\mathbb{P} &= \mathbb{P}\Lambda\mathbb{P}(I - \tfrac{\tau}{4}\mathbb{P}\Lambda\mathbb{P})^2 \end{aligned} \tag{88}$$

c To evaluate $\mathbb{P}\Sigma\mathbb{P}$ we need to compute $\Omega P P^T \Omega$. For $i = 1 \ldots N'$ and $k = 1 \ldots N$ we have

$$(P^T\Omega)_{ik} = \frac{1}{2}\left(S_{2i-1,k} + 2S_{2i,k} + S_{2i+1,k}\right)$$

Hence, since $\Omega P P^T \Omega = (P^T\Omega)^T P^T \Omega$, we have

$$\begin{aligned} (\Omega P P^T \Omega)_{jk} &= \frac{1}{4}\sum_{i=1}^{N'} \left(S_{2i-1,j} + 2S_{2i,j} + S_{2i+1,j}\right)\left(S_{2i-1,k} + 2S_{2i,k} + S_{2i+1,k}\right) \\ &= \frac{2h}{4}\sum_{i=1}^{N'} s_{2i-1,j}\left(s_{2i-1,k} + s_{2i,k} + s_{2i+1,k}\right) \\ &\quad + 2s_{2i,j}\left(s_{2i-1,k} + s_{2i,k} + s_{2i+1,k}\right) \\ &\quad + s_{2i+1,j}\left(s_{2i-1,k} + s_{2i,k} + s_{2i+1,k}\right) \end{aligned}$$

where we have set $S_{jk} = \sqrt{2h}s_{jk} = \sqrt{2h}\sin(j\theta_k)$. Using the formula

$$\sin(a-b) + \sin(a+b) = 2\sin(a)\cos(b) \tag{89}$$

we have

$$\begin{aligned} s_{2i-1,j} + s_{2i+1,j} &= \sin(2i\theta_j - \theta_j) + \sin(2i\theta_j + \theta_j) \\ &= 2\sin(2i\theta_j)\cos(\theta_j) \\ &= 2s_{ij}\cos(\theta_j) \end{aligned}$$

hence

$$(\Omega PP^T\Omega)_{jk} = h(1+\cos\theta_j)\sum_{i=1}^{N'} s_{2i,j}\left(s_{2i-1,k} + s_{2i,k} + s_{2i+1,k}\right).$$

Using the definition of $\tilde{\sigma}_{jk}$ in (74) and because $\Omega PP^T\Omega$ is symmetric, we have

$$(\Omega PP^T\Omega)_{jk} = 2h\cos^2\left(\tfrac{\theta_j}{2}\right)\begin{cases} \tilde{\sigma}_{jk} & 1 \le j \le N', \quad \forall k \\ \tilde{\sigma}_{kj} & 1 \le k \le N', \quad \forall j \\ \frac{1}{h}\cos^2\left(\frac{\theta_k}{2}\right) & N'+2 \le j = k \le N \\ 0 & \text{else} \end{cases}$$

According to (76) that gives the values of $\tilde{\sigma}_{jk}$ for $j = 1 \ldots N'$ and $k = 1 \ldots N$ we get

$$(\Omega PP^T\Omega)_{jk} = \begin{cases} 2\cos^4\left(\frac{\theta_k}{2}\right) & 1 \le j = k \le N, \quad j,k \ne N'+1 \\ -2\cos^2\left(\frac{\theta_j}{2}\right)\cos^2\left(\frac{\theta_k}{2}\right) & j+k = N+1, \quad j,k \ne N'+1 \\ 0 & \text{else} \end{cases}$$

and

$$(\mathbb{P}\Sigma\mathbb{P})_{jk} = \frac{\delta_{jk}}{\lambda_{N+1-k}} - \frac{1}{4}(\Omega PP^T\Omega)_{jk} \tag{90}$$

With

$$\lambda_{N+1-k} = 4 + 2\cos(\theta_{N+1-k}) = 4 - 2\cos\theta_k$$

we finally have

i) $j = k$ and $j,k \ne N'+1$

$$(\mathbb{P}\Sigma\mathbb{P})_{jk} = \frac{1-\cos^4(\frac{\theta_k}{2})(2-\cos\theta_k)}{4-2\cos\theta_k}$$

ii) $j = k = N'+1$

$$(\mathbb{P}\Sigma\mathbb{P})_{jk} = \frac{1}{\lambda_{N'+1}} = \frac{1}{4}$$

iii) $j + k = N+1$ and $j,k \ne N'+1$

$$(\mathbb{P}\Sigma\mathbb{P})_{jk} = \frac{1}{2}\cos^2(\tfrac{\theta_k}{2})\sin^2(\tfrac{\theta_k}{2})$$

iv) else

$$(\mathbb{P}\Sigma\mathbb{P})_{jk} = 0$$

It follows that the filling structure of $(\mathbb{P}\Sigma\mathbb{P})$ is the same as in the Figure 34.

d Let us compute the eigenpairs of $(\mathbb{P}\Sigma\mathbb{P})(\mathbb{P}D^2\mathbb{P})$. According to (87) the diagonal matrix $\mathbb{P}D^2\mathbb{P}$ is such that

$$\mathbb{P}D^2\mathbb{P} = \mathbb{P}\Lambda\mathbb{P}(I - \frac{\tau}{4}\mathbb{P}\Lambda\mathbb{P})^2$$

whose entries d_k^2 are

$$d_k^2 = \lambda_{N+1-k}\left(I - \frac{\tau}{4}\lambda_{N+1-k}\right)^2$$

With $\tau = \frac{4}{5}$ we have in particular

$$d_k^2 = \frac{1}{25}\lambda_{N+1-k}(1 + 2\cos\theta_k)^2$$

According to the structure of $(\mathbb{P}\Sigma\mathbb{P})(\mathbb{P}D^2\mathbb{P})$, it is obvious that the vector $\mathbf{w}_{N'+1} = \mathbf{e}_{N'+1}$ is an eigenvector associated to the eigenvalue $\alpha_{N'+1} = \frac{1}{4}d_{N'+1}^2 = \frac{1}{25}$. To obtain a closed form for the other eigenpairs we adopt the same strategy as in section 4.2.4.

Let $k \leq N'$ and consider the following ansatz for the eigenvectors $\mathbf{w}_k$ of $\mathbb{P}\Sigma\mathbb{P}\mathbb{P}D^2\mathbb{P}$: assume that $\mathbf{w}_k$ is such that $\mathbf{w}_k = x_k\mathbf{e}_k + x_{N+1-k}\mathbf{e}_{N+1-k}$. We assume w.l.o.g. that either $x_{N+1-k} = 1$ or $\mathbf{w}_k$ is normalized, *i.e.* $x_k^2 + x_{N+1-k}^2$, with $x_k \geq 0$. For each $\mathbf{w}_k$ the following linear system has to be solved:

$$(\mathbb{P}\Sigma\mathbb{P}\mathbb{P}D^2\mathbb{P})\mathbf{w}_k = \alpha_k\mathbf{w}_k.$$

Injecting the ansatz gives the system

$$\left\{\begin{array}{rcrcl} x_k(\mathbb{P}\Sigma\mathbb{P}\mathbb{P}D^2\mathbb{P})_{k,k} & + & (\mathbb{P}\Sigma\mathbb{P}\mathbb{P}D^2\mathbb{P})_{k,N+1-k} & = & \alpha_k x_k \\ x_k(\mathbb{P}\Sigma\mathbb{P}\mathbb{P}D^2\mathbb{P})_{N+1-k,k} & + & (\mathbb{P}\Sigma\mathbb{P}\mathbb{P}D^2\mathbb{P})_{N+1-k,N+1-k} & = & \alpha_k \end{array}\right.$$

whose unknowns are x_k and α_k. Hence we have defined N' linear systems. Each system can be separated into one 2nd order equation in x_k and one linear in α_k. Thus we have 2 pairs (x_k, α_k) of solutions for each system. That is, we have $2N'$ eigenpairs.

According to Maple we obtain the following result:

i) The N' non-zero linearly independent vectors

$$\begin{array}{rcl} \mathbf{w}_k & = & \left((4\sin^2(\frac{\theta_k}{2}) - 3)^2\sin^2(\frac{\theta_k}{2}) - 1\right)\mathbf{e}_k \\ & & +(4\sin^2(\frac{\theta_k}{2}) - 3)^2\sin^2(\frac{\theta_k}{2})\mathbf{e}_{N+1-k} \end{array}$$

belong to the null space. They are eigenvectors with eigenvalue $\alpha_k = 0$.

ii) The N' non-zero linearly independent vectors

$$\begin{array}{rcl} \mathbf{w}_{N'+1+k} & = & \sin^2(\frac{\theta_k}{2})(2\sin^2(\frac{\theta_k}{2}) - 3)\mathbf{e}_k \\ & & (2\sin^2(\frac{\theta_k}{2}) + 1)(\sin^2(\frac{\theta_k}{2}) - 1)\mathbf{e}_{N+1-k} \end{array}$$

are eigenvectors with eigenvalues

$$\alpha_{N'+1+k} = \frac{1}{25}\left(1 - 8\cos^2(\tfrac{\theta_k}{2})\sin^2(\tfrac{\theta_k}{2})\cos^2(\theta_k)\right)$$

All the eigenvectors $\mathbf{w}_k$ are linearly independent. Hence all eigenvectors are found.

The spectral radius of this ideal cycle is

$$\begin{array}{rcl} \rho(\mathbb{P}\Sigma\mathbb{P}\mathbb{P}D^2\mathbb{P}) & = & \max\limits_{k=1..N}|\alpha_k| \\ & = & \max\limits_{k=N'+1..N}\alpha_k \end{array}$$

If we study the function $f : \theta \mapsto 1 - 8\cos^2(\theta)\sin^2(\theta)\cos^2(2\theta)$ and its derivative on the interval $]0\ \frac{\pi}{4}[$ we can show that f is positive and bounded above by 1. Hence for all $k > N' + 1$, α_k is smaller than $\frac{1}{25}$. Since $\alpha_{N'+1} = \frac{1}{25}$ the spectral radius is given by

$$\rho(\mathbb{P}\Sigma\mathbb{P}\mathbb{P}D^2\mathbb{P}) = \alpha_{N'+1} = \frac{1}{25}. \tag{91}$$

A.5 Spectral radius of the shape optimization problem with algebraic transfer

Recall that $Q = \Omega_2$, $G_\tau = I - \frac{\tau}{4}B$ and $H_h = \beta_h B$ where $\beta_h = \frac{h}{6}$. We first examine the GCA matrix $Q^T H_h Q$:

$$\begin{aligned} Q^T H_h Q &= \beta_h \Omega_2^T \begin{bmatrix} \Omega_1 & \Omega_2 \end{bmatrix} \begin{pmatrix} \Lambda_1 & 0 \\ 0 & \Lambda_2 \end{pmatrix} \begin{bmatrix} \Omega_1^T \\ \Omega_2^T \end{bmatrix} \Omega_2 \\ &= \beta_h \begin{bmatrix} 0 & I \end{bmatrix} \begin{pmatrix} \Lambda_1 & 0 \\ 0 & \Lambda_2 \end{pmatrix} \begin{bmatrix} 0 \\ I \end{bmatrix} \\ &= \beta_h \Lambda_2. \end{aligned}$$

Hence it is easy to inverse the coarse subproblem yielding

$$\begin{aligned} \Sigma &= I - Q \left(Q^T H_h Q\right)^{-1} Q^T H_h \\ &= I - \beta_h^{-1} \Omega_2 \Lambda_2^{-1} \Omega_2^T \beta_h B \\ &= I - \Omega_2 \Lambda_2^{-1} \Omega_2^T \begin{bmatrix} \Omega_1 & \Omega_2 \end{bmatrix} \begin{pmatrix} \Lambda_1 & 0 \\ 0 & \Lambda_2 \end{pmatrix} \begin{bmatrix} \Omega_1^T \\ \Omega_2^T \end{bmatrix} \\ &= I - \Omega_2 \Lambda_2^{-1} \Lambda_2 \Omega_2^T \\ &= I - \Omega_2 \Omega_2^T \end{aligned}$$

Applying similarity transformations on G gives

$$\begin{aligned} G &= G_\tau \Sigma G_\tau \\ &= G_\tau \Omega \Omega^T \Sigma \Omega \Omega^T G_\tau \\ &\sim (\Omega^T \Sigma \Omega)(\Omega^T G_\tau \Omega)^2 \end{aligned}$$

where

$$\begin{aligned} \Omega^T \Sigma \Omega &= I - \Omega^T \Omega_2 \Omega_2^T \Omega \\ &= I - \begin{pmatrix} 0 & 0 \\ 0 & I \end{pmatrix} = \begin{pmatrix} I & 0 \\ 0 & 0 \end{pmatrix} \end{aligned}$$

and

$$\Omega^T G_\tau \Omega = I - \frac{\tau}{4}\Lambda$$

Hence G is similar to

$$G \sim \begin{pmatrix} I & 0 \\ 0 & 0 \end{pmatrix} \left(I - \frac{\tau}{4}\Lambda\right)^2 = \begin{pmatrix} \left(I - \frac{\tau}{4}\Lambda_1\right)^2 & 0 \\ 0 & 0 \end{pmatrix}$$

such that the spectral radius is given by

$$\rho(G) = \left(1 - \frac{\tau}{4} \min \Lambda_1\right)^2 = \left(1 - \frac{\tau}{4}\lambda_{N'+1}\right)^2.$$

In particular, with $\tau = \frac{4}{5}$ and recalling that $\lambda_{N'+1} = 4$ we have

$$\rho(G) = \left(\frac{1}{5}\right)^2 = \frac{1}{25}.$$

References

[1] Eyal Arian and Shlomo Ta'asan. Smoothers for optimization problems. In N. Duane Melson, T.A. Manteuffel, S.F. McCormick, and C.C. Douglas, editors, *Seventh Copper Mountain Conference on Multigrid Methods*, volume CP3339, pages 15–30, Hampton, VA, US, 1995. NASA, NASA Conference Publication.

[2] Alfio Borzì and Volker H. Schulz. Multigrid methods for PDE optimization. 2009.

[3] Achi Brandt. Multi-level adaptive solutions to boundary-value problems. *Mathematics of Computation, American Mathematical Society*, 31(138):333–390, 1977.

[4] William L. Briggs, Van Emden Henson, and Steve F. McCormick. *A Multigrid Tutorial (2nd ed.)*. Society for Industrial and Applied Mathematics, second edition, 2000.

[5] Benoît Chaigne and Jean-Antoine Désidéri. Méthodes hiérarchiques pour la conception optimale de forme d'antenne à réflecteur. Research Report 6625, INRIA, Sophia-Antipolis, France, September 2008.

[6] James W. Demmel. *Applied numerical linear algebra*. Society for Industrial and Applied Mathematics, Philadelphia, PA, USA, 1997.

[7] Jean-Antoine Désidéri. *Modèles discrets et schémas itératifs. Application aux algorithmes multigrilles et multidomaines.* Hermès, 1998.

[8] Jean-Antoine Désidéri. Two-level ideal algorithm for parametric shape optimization. pages 65–85. Institute of Numerical Mathematics, Rusian Academy of Sciences, 2006. Proc. of two International Conferences: Moscow, Institute of Numerical Mathematics, Russian Academy of Sciences, Sept. 16-17, 2006 and Houston, 2006.

[9] Thomas Dreyer, Bernd Maar, and Volker H. Schulz. Multigrid optimization in applications. *Journal of Computational and Applied Mathematics*, 120(1-2):67–84, 2000.

[10] Gerald Farin. *Curves and Surfaces for CAGD: a practical guide*. Morgan Kaufmann Publishers Inc., San Francisco, CA, USA, fifth edition edition, 2002.

[11] R.P. Fedorenko. A relaxation method for solving elliptic difference equations. *Russian Journal of Computational and Applied Mathematics*, 1:1092–1096, 1961.

[12] R.P. Fedorenko. The speed of convergence of one iterative process. *USSR Computational Mathematics and Mathematical Physics*, 4(3):227–235, 1964.

[13] Wolfgang Hackbusch. *Multigrid Methods and Applications*. Springer-Verlag, New York, U.S., 1985.

[14] Robert Michael Lewis and Stephen G. Nash. A multigrid approach to the optimization of systems governed by differential equations. In *8th AIAA/USAF/NASA/ISSMO Symposium on Multidisciplinary Analysis and Optimization*, Long Beach, CA, US, 2000. AIAA.

[15] Robert Michael Lewis and Stephen G. Nash. Model problems for the multigrid optimization of systems governed by differential equations. *SIAM J. Sci. Comput.*, 26(6):1811–1837, 2005.

[16] Nathalie Marco and François Beux. Multilevel optimization: Application to one-shot shape optimum design. Research Report 2068, INRIA, Sophia-Antipolis, France, 1993.

[17] Nathalie Marco and Alain Dervieux. Multilevel parameterization for aerodynamical optimization of 3d shapes. Research Report 2949, INRIA, Sophia-Antipolis, France, July 1996.

[18] Massimiliano Martinelli and François Beux. Multi-level gradient-based methods and parametrisation in aerodynamic shape design. *Revue Européenne de Mécanique Numérique*, 17(1-2):169–197, 2008.

[19] Bijan Mohammadi and Olivier Pironneau. *Applied Shape Optimization for Fluids*. Oxford University Press, England, 2001.

[20] Stephen G. Nash. A multigrid approach to discretized optimization problems. *Optimization Methods and Software*, 14:99–116, 2000.

[21] Olivier Pironneau and Elijah Polak. Consistent approximations and approximate functions and gradients in optimal control. *SIAM Journal on Control and Optimization*, 41(2):487–510, 2002.

[22] Elijah Polak. *Optimization: algorithms and consistent approximations*. Springer-Verlag New York, Inc., New York, NY, USA, 1997.

[23] J. W. Ruge and K. Stuben. *Algebraic Multigrid*, chapter 4, pages 73–130. SIAM, Philidelphia, Pennsylvania, 1987.

[24] Volker H. Schulz. Solving discretized optimization problems by partially reduced sqp methods. *Computing and Visualization in Science*, 1(2):83–86, 1998.

[25] Peter Wesseling. *An Introduction to Multigrid Methods*. John Wiley & Sons, 1991.

[26] Ji Chao Zhao, Jean-Antoine Désidéri, and Badr Abou el Majd. Two-level correction algorithms for model problems. Research Report 6246, INRIA, Sophia-Antipolis, France, July 2007.

Centre de recherche INRIA Sophia Antipolis – Méditerranée
2004, route des Lucioles - BP 93 - 06902 Sophia Antipolis Cedex (France)

Centre de recherche INRIA Bordeaux – Sud Ouest : Domaine Universitaire - 351, cours de la Libération - 33405 Talence Cedex
Centre de recherche INRIA Grenoble – Rhône-Alpes : 655, avenue de l'Europe - 38334 Montbonnot Saint-Ismier
Centre de recherche INRIA Lille – Nord Europe : Parc Scientifique de la Haute Borne - 40, avenue Halley - 59650 Villeneuve d'Ascq
Centre de recherche INRIA Nancy – Grand Est : LORIA, Technopôle de Nancy-Brabois - Campus scientifique
615, rue du Jardin Botanique - BP 101 - 54602 Villers-lès-Nancy Cedex
Centre de recherche INRIA Paris – Rocquencourt : Domaine de Voluceau - Rocquencourt - BP 105 - 78153 Le Chesnay Cedex
Centre de recherche INRIA Rennes – Bretagne Atlantique : IRISA, Campus universitaire de Beaulieu - 35042 Rennes Cedex
Centre de recherche INRIA Saclay – Île-de-France : Parc Orsay Université - ZAC des Vignes : 4, rue Jacques Monod - 91893 Orsay Cedex

Éditeur
INRIA - Domaine de Voluceau - Rocquencourt, BP 105 - 78153 Le Chesnay Cedex (France)
http://www.inria.fr
ISSN 0249-6399